Convergent evolution of monocyte differentiation in adult skin permits repair of the Langerhans cell network

Anna Appios[1,a], James Davies[1,a], Sofia Sirvent[2,a], Stephen Henderson[3], Sébastien Trzebanski[4], Johannes Schroth[5], Morven L. Law[5], Inês Boal Carvalho[1], Howard Yuan-Hao Kan[3], Christina Major[6,7], Andres Vallejo[2], Nigel J. Hall[6,7], Michael Ardern-Jones[6,8,9], Sian M. Henson[5], Elaine Emmerson[10], Steffen Jung[4], Marta E. Polak[2,9]✉, and Clare L. Bennett[1]✉

[1]Department of Haematology, UCL Cancer Institute, University College London, 72 Huntley Street, London WC1E 6DD, UK.
[2]Systems Immunology Group, Clinical and Experimental Sciences, Faculty of Medicine, University of Southampton; Southampton, UK.
[3]Bill Lyons Informatics Centre, Cancer Institute, University College London, London WC1E 6DD, UK.
[4]Department of Immunology and Regenerative Biology, Weizmann Institute of Science, Rehovot 76100, Israel.
[5]William Harvey Research Institute, Barts & The London School of Medicine and Dentistry, Queen Mary University of London, Charterhouse Square, London EC1M 6BQ UK.
[6]University Hospital Southampton NHS Foundation Trust, Southampton, UK.
[7]Human Development and Health, Faculty of Medicine, University of Southampton; Southampton, UK.
[8]Dermatopharmacology, Clinical and Experimental Sciences, Faculty of Medicine, University of Southampton; Southampton, UK.
[9]Institute for Life Sciences, University of Southampton; Southampton, UK.
[10]University of Edinburgh, Little France, Edinburgh
[a]These authors contributed equally to this work

Abstract

Langerhans cells (LCs) are a unique population of phagocytes programmed within embryonic skin to maintain tissue and immunological homeostasis at the epidermal barrier site. Unique amongst tissue-resident macrophages, LCs play roles in skin innervation and repair, while also functioning as migrating professional antigen presenting cells, a capability classically assigned to dendritic cells (DC). We currently lack insight into the molecular pathways that determine this dichotomy, when they are established, and whether precursors recruited to the adult skin niche access the same instructive signals laid down *in utero*. Tracking differentiation of monocyte-derived (m)LCs after destruction of embryo-derived cells in murine adult skin, we reveal intrinsic intra-epidermal heterogeneity and selection of MDP-monocytes to by-pass gene programs specifying a macrophage fate. Within the adult skin, we demonstrate that the hair follicle niche provides Notch signals that determine commitment to become resident mLCs. Using a unique human LC dataset, we show that embryo-derived (e)LCs in newborn human skin retain transcriptional evidence of their macrophage origin, but this is superseded by distinct DC-like immune modules after expansion of the eLC network. Thus, convergent differentiation of monocytes within adult skin replicates conditioning of eLC towards more immunogenic DC-like cells within post-natal skin.

Langerhans cells | monocytes | epidermis | skin | bone marrow transplant
Correspondence: ***c.bennett@ucl.ac.uk, M.E.Polak@soton.ac.uk***

Introduction

Langerhans cells (LCs) are a unique and highly conserved population of mononuclear phagocytes that reside in the outer epidermis of the skin. Initially defined as prototypic dendritic cells (DCs) due to their potential to migrate to draining lymph nodes (LNs) and initiate T cell immunity (Jakob and Udey, 1999), subsequent fate mapping studies supported a common origin with tissue macrophages in other organs (Mass *et al.* 2016). As such, LCs are the only resident macrophage population that acquires the DC-like ability to migrate out of the tissue, and this dual nature is reflected in the breadth of LC function in the skin LNs: as DC-like cells, LCs control T cell tolerance and function in LNs and the skin (Kaplan, 2017); by comparison, unlike DCs, LCs depend on CSF1R signalling for survival (Ginhoux *et al.* 2006), and there is increasing data to support more macrophage-like functions via interaction with peripheral nerves (Zhang *et al.* 2021) and promotion of angiogenesis during wound healing (Wasko *et al.* 2022). But the signals that control this functional dichotomy within the spatial context of intact skin remain poorly defined.

Entry of LC precursors into the BMP7- and TGFβ-rich environment of the epidermis results in activation of a Runx3- and Id2-dependent program of differentiation (Mass *et al.* 2016; Kaplan, 2017; Strobl, Krump and Borek, 2019), defined by expression of the c-type lectin Langerin (CD207) and high expression of cell adhesion molecules including EpCAM and E-cadherin. Once resident, eLCs depend on IL-34 for survival (Greter *et al.* 2012; Wang *et al.* 2012) and the network is maintained throughout life via local proliferation of mature LCs (Merad *et al.* 2002, 2004), independent of the adult circulation. Murine fetal macrophage precursors expressing the quintessential protein CX3CR1, enter the early embryonic skin and differentiate into LC-like cells within this environment (Hoeffel *et al.* 2012; Mass *et al.* 2016), but don't mature into bona fide embryo-derived (e)LCs until after birth (Tripp *et al.* 2004; Chorro *et al.* 2009). By contrast, human eLCs differentiate within the epidermis before birth and histologically resemble adult cells by an estimated gestation age of 18 weeks (Meindl *et al.* 2009; Elbe-Bürger and Schuster, 2010). In both mice and humans, eLC numbers are sparse at birth and the epidermis becomes fully populated following a proliferative burst within the first week of exposure to the external environment in mice (Chorro *et al.* 2009), and within 2 years of age in humans (Meindl *et al.* 2009), but we

do not know if or how this transition may shape eLC identity and function.

Tissue-resident macrophage identity is largely imprinted by the local anatomical niche wherein instructive signals permit differentiation and survival of long-lived, specialized resident cells (T'Jonck, Guilliams and Bonnardel, 2018). Environmental signals determine cellular identity via epigenetic regulation of specific transcription factor networks (Gosselin *et al.* 2014; Lavin *et al.* 2014), controlled by the transcription factor Zeb2 which is required for the expression of the unique gene programs that define identity and function within tissues (Scott *et al.* 2018; Anderson *et al.* 2021). These niches have been carefully delineated in tissues such as the lungs and liver where interaction with local epithelia supports differentiation of resident macrophage populations (Bonnardel *et al.* 2019; McCowan *et al.* 2021). However, recent evidence suggests that heterogeneity within classical Ly6C$^+$ monocytes results in some intrinsic bias in the cells that contribute to tissue-resident macrophage populations (Yáñez *et al.* 2017; Kwok *et al.* 2020). For instance, whilst all monocytes give rise to gut macrophages, in the lung granulocyte-macrophage progenitor (GMP)-derived monocytes preferentially became Lyve1$^+$MHCII^{low} interstitial macrophages but monocyte-dendritic cell progenitor (MDP)-derived monocytes seeded the Lyve1^{neg}MHCII^{high} population (Trzebanski *et al.* 2023). These data suggest that ontogeny may also shape tissue macrophage differentiation.

The epidermis is composed of layers of stratified epithelial cells which are interspersed in non-glabrous skin with follicular structures that support the cycles of hair growth. Within follicular epithelial cells tightly demarcated areas of CCL2 expression at the upper follicular isthmus is associated with recruitment of monocytes to the epidermis (Nagao *et al.* 2012), which is spatially distinct from sites of integrin αvβ6 expression required for activation of latent TGFβ and retention of mature LCs in the interfollicular epidermis (Mohammed *et al.* 2016). MHCII$^+$CD11b$^+$ cells accumulated around hair follicles upon induction of inflammation in LC-depleted bone marrow (BM) chimeras, and LC repopulation was impaired in mice lacking hair follicles (Nagao *et al.* 2012). But whether the hair follicle site provides a differentiation niche, or merely serves as a point of entry for monocytes into the epidermis is not known, and we do not understand how the epidermal environment programs differentiation of the unique macrophage-DC state in LCs.

Pathological destruction of the eLC network during graft-versus-host disease (GVHD) results in replacement of eLCs with donor bone marrow (BM)-derived LCs (Collin *et al.* 2006; Mielcarek *et al.* 2014). We and others have shown that acute inflammation and destruction of eLCs in murine models of GVHD or UV irradiation triggers influx of monocytes to the epidermis (Ginhoux *et al.* 2006; Seré *et al.* 2012; Santos e Sousa *et al.* 2018; Ferrer *et al.* 2019). By tracking monocyte differentiation, we demonstrated that epidermal monocytes undergo differentiation to EpCAM$^+$CD207^{neg} precursors, which become long-lived EpCAM$^+$CD207$^+$ monocyte-derived (m)LCs that are transcriptionally indistinguishable from the cells they replace, are radio-resistant, and acquire DC-like functions of migration to LNs and priming of T cells (Ferrer *et al.* 2019). This model therefore provides a tractable tool with which to understand how tissue niches within the epidermis permit LC differentiation. By combining transcriptional analyses with experimental cell biology, we have investigated the mechanisms of LC instruction within the murine and human post-natal epidermis. We demonstrate an unexpected heterogeneity in monocyte fate upon entry into the inflamed epidermis, whereby some monocytes default to becoming CD206$^+$ macrophages but not LCs. We identify MDP- but not GMP-derived monocytes as mLC precursors, showing loss of Zeb2 and upregulation of EpCAM in those cells that become mLCs. Mechanistically, we identify Notch signaling within a unique adult hair follicle niche as a key factor committing monocytic precursors to the LC differentiation pathway. By exploiting a novel dataset of LCs from human newborn, infant and children's skin we demonstrate that mLC differentiation mirrors post-natal maturation of eLCs wherein proliferation after birth is linked to loss of Zeb2 and acquisition of a DC-like immune gene program. Thus, these data demonstrate that a combination of ontogeny and environmental signals provided by the adult hair follicle niche replicate post-natal LC maturation towards DC-like cells, revealing mechanisms of convergent adaptation to maintain the LC network in the skin.

Results

Single cell RNA-sequencing reveals monocyte-derived cell heterogeneity in the inflamed epidermis. To determine the molecular pathway(s) that resulted in successful tissue-residency and differentiation of mLCs in adult skin, we exploited our murine model of minor h-antigen mismatched HSCT, in which allogeneic T cells destroy resident eLCs (Merad *et al.* 2005; Santos e Sousa *et al.* 2018). In this model, mLCs replace the eLC network (Ferrer *et al.* 2019). We carried out single-cell RNA-sequencing (scRNA-seq) on sorted donor CD11b$^+$MHCII$^+$ cells isolated from the epidermis 3 weeks post-BMT with male antigen-specific Matahari (Mh) T cells (Valujskikh *et al.* 2002), using the 10X Genomics platform (Figure 1A, S1A). Analysis of the cells at this time point allowed us to map the spectrum of CD11b^{high} monocytes, CD11b^{int}EpCAM$^+$CD207^{neg} precursors and CD11b^{int}EpCAM$^+$CD207$^+$ LCs we have previously defined in the epidermis (Ferrer *et al.* 2019). Dimensionality reduction and clustering of the cells demonstrated unexpected heterogeneity between donor BM-derived cells, with several transcriptionally distinct clusters of cells around a central collection of clusters that were more similar to each other (Figure 1B). Use of significance analysis demonstrated that the data were not overfitted and therefore likely to be biologically relevant (Figure S2A)(Grabski, Street and Irizarry, 2023). Identification of the differentially expressed genes that defined the clusters (Figure 1C, S1B) revealed 3 populations of mLCs: resident (res) mLCs (*Cd207*, *Epcam*, *Mfge8*); cycling mLCs (*Top2a*, *Mki67*, but which also retained the res mLC signature); and migrating

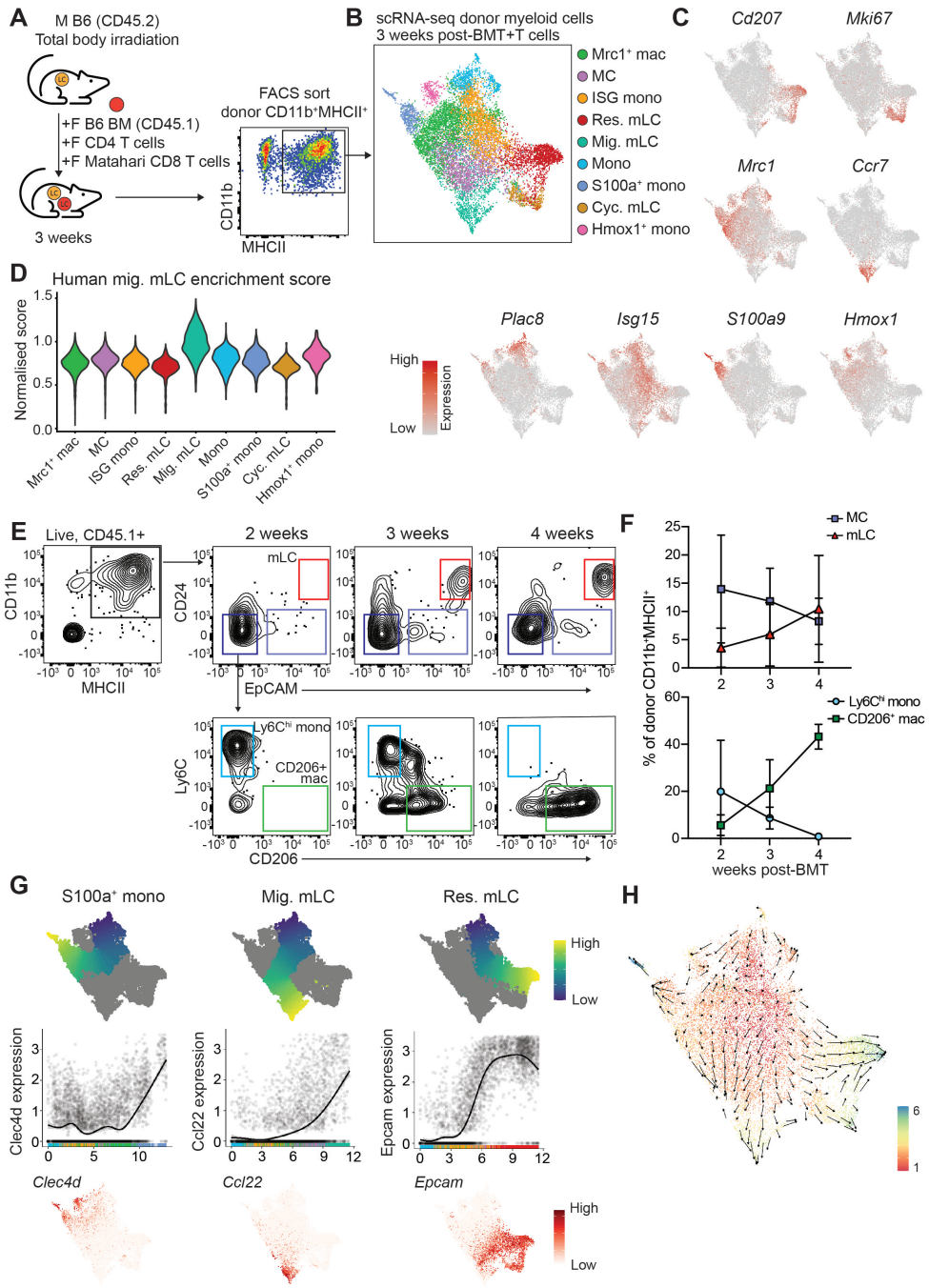

Fig. 1. scRNA-seq reveals monocyte-derived cell heterogeneity in the GVHD epidermis. A. Experimental design showing murine bone marrow transplant model and populations sorted for scRNA-seq. M, male; F, female; BM, bone marrow. For full gating strategy see figure S1A. **B.** UMAP and clustering of donor CD11b$^+$MHCII$^+$ cells analyzed by 10X scRNA-seq. Mac, macrophage; MC, monocyte-derived cell; res. mLC, resident monocyte-derived Langerhans cell; mig. mLC, migratory mLC; mono, monocyte; cyc. mLC, cycling mLC. **C.** Heatmap overlays showing expression of indicated genes across dataset. **D.** Violin plot showing enrichment scores for a human mig. LC gene signature across clusters. **E.** Representative flow plots showing donor CD11bscript+MHCII$^+$ cells from GVHD murine epidermis at the indicated time-points following BMT+T cells. Gated on live, singlets, CD45.1$^+$ (donor) cells. **F.** Quantification of populations indicated in (E). Data are represented as mean±SD, (n=2 for 2 weeks, 8 for 3 weeks, 2 for 4 weeks). Data are pooled from three independent experiments. **G.** Differentiation trajectories calculated using Slingshot overlaid onto UMAP from (B) (above), normalized expression of indicated genes (y-axis) across pseudotime (x-axis) for the indicated trajectories (middle) and feature plots showing normalized expression of indicated genes overlaid onto UMAP from (B) (below). **H.** RNA velocity analysis applied to data from (B).

(mig) mLCs (*Cd83*, *Nr4a3*, *Ccr7*). Consistent with human LC data (Sirvent *et al.* 2020; Liu *et al.* 2021; Reynolds *et al.* 2021), mig mLC downregulated genes associated with LC identity (*Cd207*, *Epcam*) and instead expressed a generic monocyte-derived DC signature (Figure 1C, S1B) that correlated with a high enrichment score for human migrating LCs (Figure 1D) (Sirvent *et al.* 2020). These data suggest that some mLCs are constitutively primed for migration as observed in human steady state eLCs (Liu *et al.* 2021). We also identified a classical monocyte cluster (Mono; *Plac8*, *Ly6c2*) likely to have recently arrived in the epidermis, and two small populations of cells that shared monocyte/neutrophil activation markers, with signs of recent oxidative stress (S100a$^+$ mono and Hmox1$^+$ mono) (Figure 1C). The central cluster of cells was resolved into three merged clusters that all shared macrophage identities with monocyte-derived cells found at other sites. The clusters that overlapped most closely with classical monocytes were defined as interferon-stimulated gene monocytes (ISG mono; *Isg15*, *Ifit2*, *Ifit3*) that were also evident in some of the classical monocyte cluster cells. Conversely, we observed a cluster of *Mrc1* (CD206)- and *Arg1*-expressing monocyte-derived macrophage-like cells (Mrc1$^+$ mac) that resemble those found in the dermis (Figure 1C, S1B) (Kolter *et al.* 2019). These cells appeared to have differentiated along a default macrophage pathway to express canonical

tissue macrophage genes and shared some similarity to the converting macrophages recently identified in the pleural cavity after nematode infection (Finlay *et al.* 2023). Intriguingly, we also detected a separate cluster of cells that were identified by their upregulation of *Ccl17*, *Mgl2*, *Dcstamp*, and *Itgax* genes linked to monocyte-derived DCs. (Figure 1C, S1B). Given the lack of clarity into the identity of these cells, we labelled them "converting monocyte-derived cells" (MC), in reference to a similar transitional population of cells recently described by the Allen lab (Finlay *et al.* 2023). Flow cytometry data validated the heterogeneous cell fates showing loss of monocytes and MC over time with expansion of mLCs and CD206$^+$ macrophages (Figure 1E, F). Analysis of eLCs co-isolated from the GVHD skin at the 3 week time-point revealed 3 clusters of cells that resembled those identified in human skin (Liu *et al.* 2021): clusters 1 and 2 were defined as resident eLCs while the third cluster mirrored *Ccl22*$^+$*Nr4a3*$^+$ migrating mLCs (Figure S2B).

To better understand which monocytes became mLCs, we inferred the trajectory of monocyte development towards finite cell states using Slingshot and RNA velocity (Figures 1G and H). These analyses revealed S100a$^+$ monocytes as a distinct cell state, likely due to direct differentiation of incoming monocytes via the Hmox1$^+$ monocyte cluster, defined by expression of *Clec4d*. A separate pathway towards migratory mLC was inferred by high expression of *Ccl22* in the absence of *Cd207* (Figures 1C and G); this distinct route is likely driven by the down regulation of *Cd207* in migratory mLC (Reynolds *et al.* 2021) resulting in the algorithm identifying these cells as a distinct cell fate. By comparison, upregulation of *Epcam* defined those monocytes destined to become resident mLCs (Figure 1G). But, whilst differentiation towards resident mLC populations was clearly defined as an endpoint in latent time (Figure 1H), arrows indicating direction of differentiation predicted by RNA velocity displayed a degree of uncertainty within Mrc1$^+$ macs and ISG monocytes which was resolved once cells enter the MC cluster, congruent with expression of *Epcam* (Figure 1G). This apparent lack of commitment was illustrated by the short latent time and relative increase in unspliced versus spliced transcripts within ISG monos and Mrc1$^+$ macs compared to committed mLC populations (Figure S2C). Focusing on differentiation towards resident mLCs, progenitor marker gene analysis demonstrated loss of monocyte-specific genes (*Ly6c2*, *Plac8*) and acquisition of LC-defining genes (*Cd207*, *Epcam*, *Mfge8*), those associated with cell adhesion (*Cldn1*) and production of non-inflammatory lipid mediators (*Ptgs1*, *Ltc4s*, *Lpar3*, *Hpgds*) (Figure S2D).

Thus, specification of a mLC fate in the adult epidermis occurs in situ in the skin, but not all monocytes receive these signals and some undergo a default macrophage differentiation. Rather than discrete points of cell fate decisions, our combined analyses reveal a continuum of genes across the central clusters which converge to program mLC development in some cells.

Monocyte ontogeny determines mLC repopulation. Heterogeneity in epidermal monocyte fate may be explained by either intrinsic bias within incoming Ly6C^{high} monocytes and/or extrinsic programming within a specified tissue niche. To test the first possibility, we investigated the epidermal monocyte population in more detail. Subsetting and re-clustering of the classical monocyte cluster revealed 3 clusters of cells (Figure 2A): most cells fell into clusters 1 and 2 while a small number of cells were grouped in cluster 3 (Figure 2B). Enrichment for gene signatures for GMP-Mos and MDP-Mos (Trzebanski *et al.* 2023), and expression of the defining genes, *Cd177* and *Slamf7* suggested that cluster 3 represented GMP-Mos, whereas clusters 1 and 2 were MDP-Mos (Figure 2C). This identification was supported by direct comparison between clusters 2 and 3; cluster 2 cells expressed higher levels of *Sell* (encoding CD62L) and classical monocyte genes (*Plac8*, *Ly6a2*), whereas cluster 3 expressed *C1q* genes and *H2-Aa*, associated with MDP-Mos (Figure 2D). To better understand the macrophage/DC potential within monocyte subsets we compared expression of a defined panel of genes (Figure 2E): cluster 3 (GMP-Mos) appeared more macrophage-like with higher expression of the glutathione reductase (*Gsr*) and *Cx3cr1*; clusters 1 and 2 were distinguished by increased, but differential, expression of *Id2*, *Mgl2*, and *Batf3* suggesting a closer relationship with DC-like cells (Figure 2E). Notably, *Mgl2* and *Ccl17*, markers of MDP-Mo progeny in the lung (Trzebanski *et al.* 2023) were expressed within MDP-Mo clusters (Figures 2E and S3A) and were also defining genes in our MC cluster from the 10X dataset (Figure S1B).

These data suggested that MDP-Mo were more likely to give rise to mLCs. Therefore, to test whether different monocytic precursors were intrinsically biased towards becoming mLC, we FACS-isolated GMP, MDP or total Ly6C$^+$ monocytes from murine BM and cultured these cells with GM-CSF, TGFβ and IL-34 to promote generation of CD24$^+$EpCAM$^+$ mLC-like cells (Figure S3B) (Chopin *et al.* 2013; Tabib *et al.* 2018; Ferrer *et al.* 2019). Figure 2E demonstrates that MDP, but not GMP, generated mLCs, in culture, replicating differentiation of total Ly6C$^+$ monocytes.

Together, these data highlight cell intrinsic differences in circulating monocytes, whereby only those cells biased along an MDP-Mo / monocyte-derived DC outcome were destined to become mLCs.

Metabolic adaptation of resident mLC, but not Mrc1$^+$ macrophages, within the epidermis. To investigate the molecular pathways involved in mLC differentiation we used SCENIC (Single Cell Regulatory Network Inference and Clustering) analysis (Aibar *et al.* 2017) to infer transcription factor-target gene groups (regulons) which were more highly active in resident mLCs than other populations, and which best explained expression of the most highly upregulated genes in our mLC cluster. Regulons enriched within resident mLC included *Zeb1* or *Rxra* and *Srebf2*, transcription factors known to be upregulated in response to hypoxia and a lipid rich environment respectively (Figure 3A) (Lengqvist et al., 2004; Bommer and MacDougald, 2011; Joseph et al., 2015). These data suggested that, in addition to intrinsic programming of LC precursors, adaptation to the unique epi-

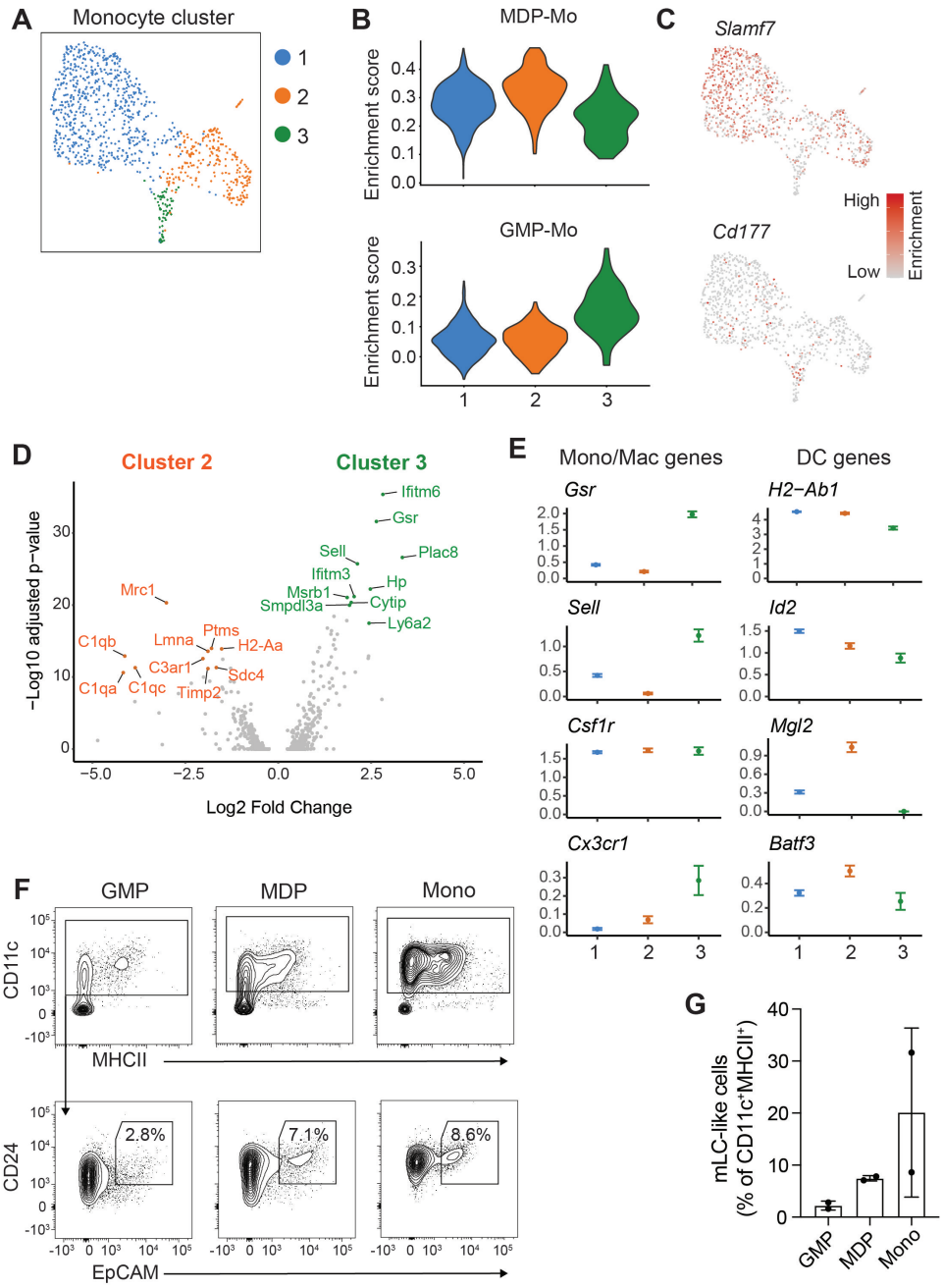

Fig. 2. Intrinsically programmed DC-biased monocytes give rise to mLC. A. UMAP and sub-clustering of monocytes from GVHD epidermis. **B.** Violin plots showing enrichment scores for MDP-Mo (above) and GMP-Mo (below) gene signatures across clusters from (A). **C.** Heatmap overlays showing normalized expression of indicated genes. **D.** Volcano plot showing DEGs between cluster 2 and cluster 3 from (A). Top 10 significant DEGs are highlighted. **E.** Scatter plot of selected genes across monocyte clusters. **F** Representative flow plots showing GMP (left), MDP (middle) and monocytes (Mono, right) that were cultured for 6 days in the presence of GM-CSF, TGFβ and IL34. Gated on live, singlets, CD45$^+$ cells. **G.** Bar graph showing the frequency of CD24$^+$EpCAM$^+$ cells identified in (D). Data are represented as mean±SD (n=2 independent experiments)

dermal environment informed mLC development. Therefore, we analyzed metabolic pathway usage across cell clusters using COMPASS, which identifies cellular metabolic states using scRNA-seq data and flux balance analysis (Wagner *et al.* 2021)(Figure 3B). These data revealed that, compared to mLCs, EpCAM$^+$ MC metabolism was dominated by use of amino acid pathways including tryptophan. Strikingly, differentiated mLCs displayed a markedly different metabolic pathway to Mrc1$^+$ macrophages, despite localisation within the same epidermal site. Consistent with long-term residency in the epidermis, and adaptation to a lipid-rich environment, mLC metabolism was dominated by fatty acid oxidation and synthesis (Bennett and Perona-Wright, 2023; Wculek *et al.* 2023).

Thus, these data suggest that transcription factor-dependent regulation of monocytes in response to the unique epidermal environment may permit long-term survival of mLCs, but not monocyte-derived macrophages.

Differentiating monocytes lose Zeb2-mediated macrophage identity to become mLCs but this does not require Ahr signaling. Analysis of the transcription factors predicted to explain the pseudo-trajectory from monocytes to resident mLCs revealed that differentiation was dominated by loss of the tissue macrophage-determination factor *Zeb2* (Figure 4A). Expression of *Zeb2* was mutually exclusive to *Epcam*-expressing cells (Figures 4B, C), suggesting that, unlike other resident macrophage populations, a Zeb2-mediated macrophage fate is suppressed during specification of mLCs. Epidermal monocytes also down-

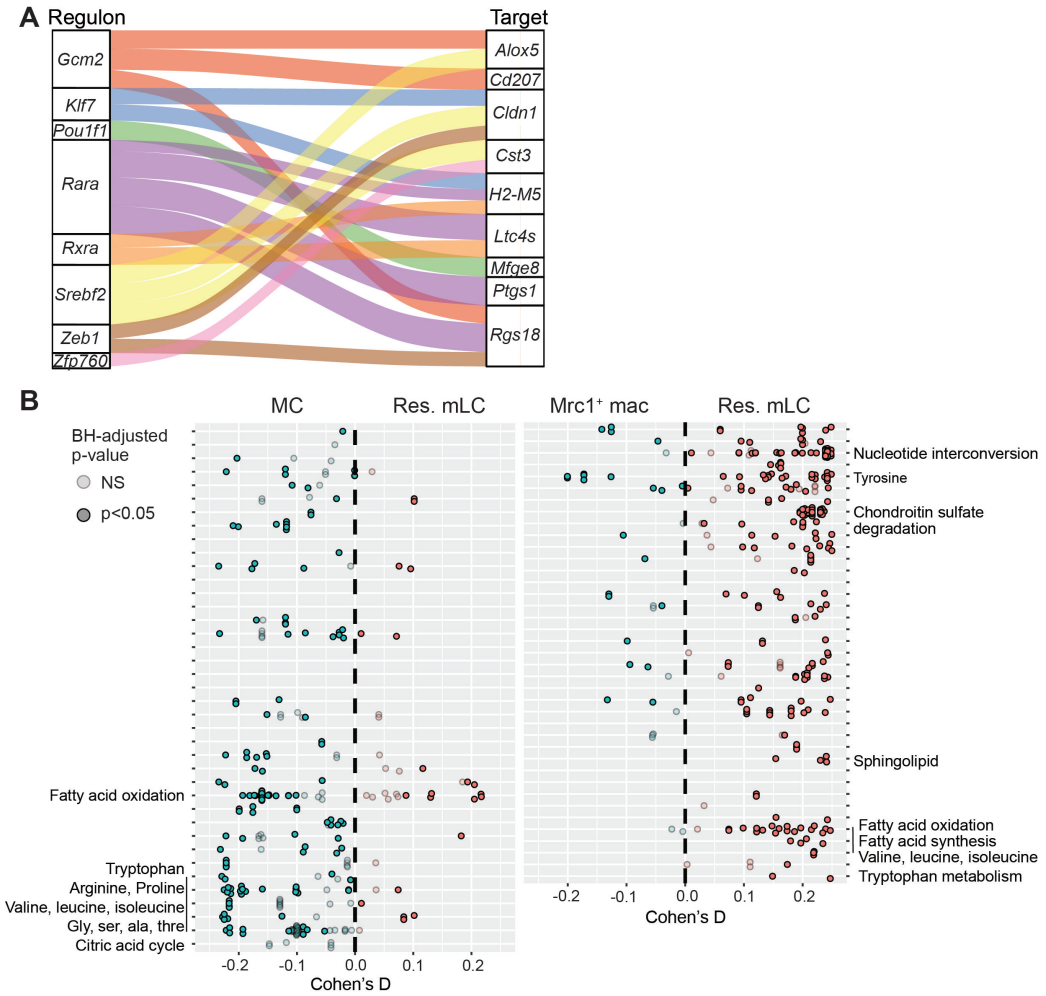

Fig. 3. Metabolic adaptation of resident mLC. A. Relationship between identified SCENIC regulons enriched in res. mLC (left) and res. mLC signature genes (Targets; right). **B.** Differential activity of metabolic reactions between MC and res. mLC (left) and Mrc1^{+} mac and res. mLC (right) analysed using COMPASS. Reactions (dots) are coloured by the sign of their Cohen's D statistic, bright dots P<0.05

regulated expression of *Klf6*, linked to pro-inflammatory gene expression and therefore consistent with emergence of quiescent LCs (Goodman *et al.* 2016), as well as the transcription factors *Fos* and *Stat1*. Notably, *Zeb2* was highly negatively correlated with expression of the LC-defining transcription factors *Id2* and the aryl hydrocarbon receptor (*Ahr*) that are also upregulated by eLCs *in utero* (Mass *et al.* 2016) (Figures 4 A-C). Mirroring DCs that migrate out of the skin, migratory mLCs were defined by upregulation of *Irf4*, *Rel* and *Nr4a3* (Figure S4A)(Baratin *et al.* 2015; Sirvent *et al.*, 2020; Reynolds *et al.* 2021; Davies *et al.*, 2022).

Previous work has shown that monocyte expression of Ahr biases differentiation towards moDCs rather than moMacs (Goudot *et al.* 2017). Ahr is not required for eLC development from pre-macrophages *in utero* (Figure S4B,C) (Esser, Rannug and Stockinger, 2009), but we questioned whether Ahr signaling could be important for MDP-Mo differentiation to mLCs in adult skin. Supporting this we also observed expression of Ahr by a small number of MCs, potentially indicating those cells en route to becoming mLCs (Figures 4D,E). To test whether Ahr signaling was required for monocyte differentiation *in vitro*, we generated mLCs in the presence or absence of the Ahr inhibitor SR1 or the agonist FICZ (Goudot *et al.* 2017). Both *Ahr* and *Cyp1b1* were augmented in EpCAM^{+} cells compared to EpCAM^{neg} cells in the presence of the agonist FICZ (Figure 4F), but activation of Ahr signaling did not result in an increase in the frequency of EpCAM^{+} mLC-like cells, probably due to Ahr ligands already present in culture media (Figures 4G and S4D) (Rannug and Fritsche, 2006). By contrast, inhibition of Ahr signaling ablated differentiation of EpCAM^{+} cells, demonstrating a requirement for mLC development *in vitro* (Figure 4G and S4D). Therefore, guided by these data we tested the requirement for Ahr *in vivo*. Exploiting the expression of Id2 and Langerin by LCs, we exploited Id2^{BFP} (Figure S4E,F)(Walker *et al.* 2019) and Langrin^{GFP} (Ferrer *et al.* 2019) reporter mice to generate competitive chimeras in which irradiated Langerin^{GFP}.B6 males received a 1:1 mix of BM from female Ahr-replete (Ahr$^{+/+}$.Id2^{BFP}.B6 reporter mice) or Ahr-deficient (Ahr$^{-/-}$.B6) donors with Matahari T cells (Figure 4H). Three weeks later the epidermis was analyzed for presence of mLCs and precursor populations. Consistent with the requirement for Ahr in CD4^{+} T cells (Esser, Rannug and Stockinger, 2009), Ahr-deficient BM cells did not contribute to repopulating splenic CD4^{+} T cells in chimeras (Figure 4I). We observed a slight bias towards Ahr-competent CD11b^{+} cells in the spleen across experiments (Figure 4I), however this ratio of Ahr-deficient to Ahr replete cells was maintained within our epidermal cells (Figure 4J). Therefore, these data demonstrated that Ahr sig-

naling was not required for mLC differentiation *in vivo*.

Together these data suggest that loss of Zeb2 is a critical step for differentiation of mLCs. But, whilst Ahr signaling was required for monocyte differentiation *in vitro*, regulation by Ahr did not determine a mLC fate within adult skin.

A unique follicular keratinocyte niche controls differentiation of mLCs. To understand the signals which regulated the transition from loss of a Zeb2-linked macrophage program to commitment to a LC identity, we next sought to define the mLC niche *in vivo*. Imaging of the skin after BMT with T cells revealed clustering of MHCII$^+$ cells around hair follicles, an anatomical site previously associated with monocyte recruitment to the epidermis (Figure 5A)(Nagao *et al.* 2012). Therefore, to define where and how monocytes differentiated within potential epidermal niches we sorted CD45^{neg} keratinocytes (Figure S5) and CD11b$^+$MHCII$^+$ cells from the same epidermal samples 3 weeks post-BMT with T cells, performed scRNA-seq using the 10X platform and batched the data with our existing CD11b$^+$MHCII$^+$ epidermal dataset. Visualization of CD45^{neg} cells by UMAP, with differential gene analysis and cross-reference to a published mouse scRNA-seq epidermal dataset (Joost *et al.* 2016) identified interfollicular epidermis-derived basal cells (*Krt14*^{high}, *Krt5*^{high}) and terminally-differentiated (*Krt10*^{high}) epidermal cells of the stratum spinosum, as well as a cluster that combined *Krt79*^{high} *Krt17*^{high} cells of the upper hair follicle with a small sub-cluster of *Mgst1*$^+$ cells that were likely to come from the sebaceous gland (Figures 5B, C and S5B). Two other clusters were identified as cycling cells (*Mki67*) and putative *Cdc20*$^+$ stem cells. To predict which keratinocytes could support differentiation of epidermal monocytes we analyzed expression of factors known to be required for monocyte or mLC survival (*Csf1*, *Il34*, *Bmp7*) and residency (*Tgfb1* and *2*, *Epcam*) (Kaplan, 2017). Figure 5D shows that while *Csf1* was not expressed by epidermal keratinocytes, *Il34*, which also binds the Csf1 receptor, was localized to Krt10$^+$ terminally-differentiated cells, consistent with its role as a survival factor for the mature LC network within the interfollicular epidermis. We could only detect low levels of *Tgfb1* and *2* and *Bmp7* transcripts which may be due to lack of activation of TGFβ at this time point in GVHD skin but may also reflect poor detection of these genes at 10X sequencing depths. By contrast, *Epcam* was specifically expressed by Krt79^{high} Krt17^{high} upper hair follicle cells. Expression of the cell adhesion molecule EpCAM, is associated with residency of monocytes within the alveolar space and differentiation to alveolar macrophages (McCowan *et al.* 2021), and EpCAM expression demarcates isthmus region epithelial cells of the upper hair follicle which express CCL2 (Nagao *et al.* 2012). Therefore, we postulated that this localized area may provide a niche for differentiating EpCAM$^+$ LC precursors. Protein analysis demonstrated high levels of EpCAM on follicular epithelium, which was transiently decreased at the peak of T cell-mediated pathology in this model (Figure 5E,F) (Santos e Sousa *et al.* 2018; Ferrer *et al.* 2019), suggesting that adhesion to this niche could contribute to the bottleneck in mLC differentiation that we observed in our previous study (Ferrer *et al.* 2019). Using the LIANA software (Dimitrov *et al.* 2022), we predicted potential interactions between monocytes, MCs and resident mLCs and the Krt79^{high}Krt17^{high} EpCAM$^+$ follicular cluster. This analysis confirmed that follicular epithelial cells were most likely to signal towards differentiating monocytes (Figure 5G), rather than established mLCs resident within the IL-34-rich interfollicular cells. Assessment of key receptor-ligand interactions identified several potential interactions via *Apoe* from follicular epithelial cells (Figure 5H), again consistent with the need for monocytes to adapt to the lipid-rich epidermal environment (Tacke *et al.* 2007). Of potential recruitment pathways, the *Cxcl14-Cxcr4* axis was predominantly located to monocytes, in agreement with previous work from the Moser lab showing CXCL14-mediated recruitment of human monocytes to the epidermis before differentiation to mLCs (Schaerli *et al.* 2005). In addition, follicular epithelial cells uniquely provided Jagged-1 and -2 (*Jag1*, *Jag2*) ligands to initiate Notch signaling in monocytes and, to a lesser extent, MCs (Figures 5H,I).

These data therefore reveal a precise and spatially restricted hair follicle niche that permits not only recruitment, but potentially differentiation of monocytes to resident mLCs in the adult epidermis.

Notch signaling is sufficient to program mLC differentiation. Our data suggested a working model in which recruitment of monocytes to the upper follicular epidermis initiates a molecular cascade that results in loss of Zeb2 but niche-dependent activation of Notch, resulting in the differentiation of CD207$^+$EpCAM$^+$ Ahr-expressing mLCs. To define mechanistic pathways leading to a mLC fate in the adult skin we first tested the impact of Notch signaling on monocytes. Provision of Jagged-1 (Jag1), but not the Notch ligand Delta-like 4 (DL4), was sufficient to enhance differentiation of monocytes towards EpCAM$^+$ mLC-like cells *in vitro* in the absence of TGFβ and IL-34 (Figure 6A). We noted that DL4 appeared to inhibit mLC development in these cultures (Figure 6A). Whilst Notch signaling did not augment mLC frequencies beyond that induced by TGFβ and IL-34 (Figure 6A) we observed selection of a mLC-fate at the expense of other default monocyte-derived macrophage- or DC-like cells indicated by expression of CD11c and CD206/CD64. (Figure 6B). Therefore, to determine the effect of Notch signaling combined with other environmental signals in the skin we cultured monocytes with GM-CSF/TGFβ/IL-34 with or without Jag1, the Ahr agonist FICZ, or both, and compared the transcriptional changes within sorted CD11b^{low}EPCAM$^+$ mLC-like cells (Figures 6C and S6A). Figures 6D and E show that cells were clustered by stimulation with considerable overlap between groups. Activation of Ahr signaling did not markedly distinguish clusters along principal component (PC) 1 and over-laid the impact of Jag1, likely due to the dominant activation of the Ahr-responsive gene *Cyp1a1* (Figure 6E). However, provision of Jag1 signaling alone led to a marked transcriptional separation suggesting fundamental reprogramming of EpCAM$^+$ cells in this group. Comparison to our *in vivo* gene signatures demonstrated that Notch sig-

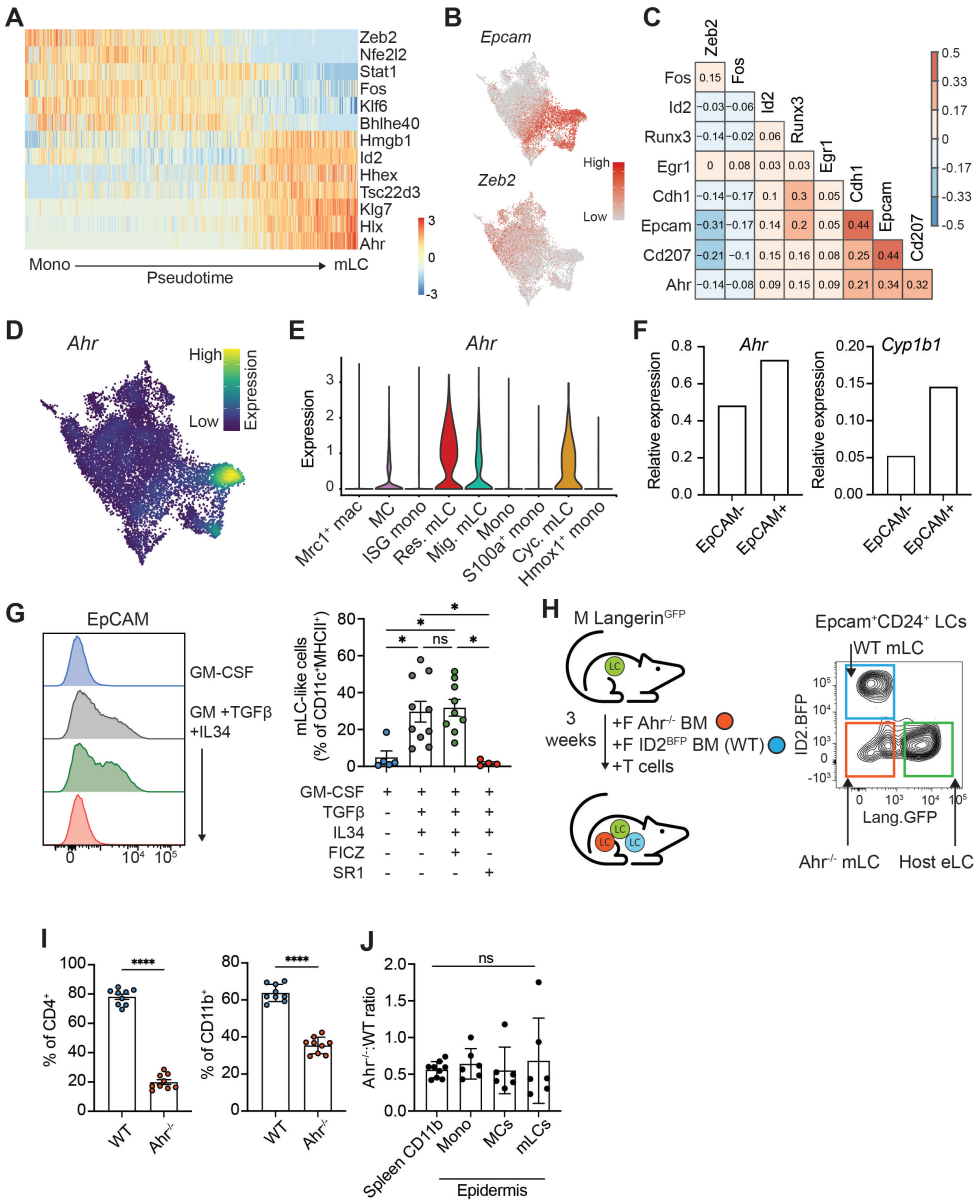

Fig. 4. mLC differentiation is associated with loss of Zeb2 and upregulation of Ahr. **A.** Heatmap showing scaled gene expression of transcription factors that are differentially expressed along the differentiation trajectory (Pseudotime) from monocyte to res. mLC. **B.** Heatmap overlays showing normalized expression of indicated genes across cells from figure 1B. **C.** Correlation of LC defining genes (y-axis) in res. mLC against expression of indicated genes across all other clusters from scRNA-seq dataset. **D.** Density plot showing expression of Ahr across cells from scRNA-seq dataset. **E.** Violin plot showing normalized expression of Ahr across clusters from scRNA-seq dataset. **F.** Relative expression of *Ahr* and *Cyp1b1* in CD11b$^+$EpCAM$^-$ and CD11b$^+$EpCAM$^+$ cells generated *in vitro* in the presence of FICZ. Expression is normalized to cells treated with GM-CSF+TGFβ+IL34 alone (n=2). **G.** Representative histogram (left) of EpCAM expression by monocytes cultured for 6 days under the indicated conditions and summary bar graph (right) of mLC-like cells generated from these conditions (for gating see Figure S4D). Data are represented as mean±SD (n=5 independent experiments). Statistical differences were assessed using Kruskal-Wallis test for multiple comparisons, * $p<0.05$. **H.** Experimental set up for competitive chimeras (left). Male Langerin^{GFP}.B6 mice received a 1:1 mix of BM from female Ahr-replete (Ahr$^{+/+}$.Id2^{BFP}.B6 reporter mice, WT) or Ahr-deficient (Ahr$^{-/-}$.B6) donors with Matahari T cells and donor chimerism was assessed in the epidermis and spleen 3 weeks post-transplant (right). M, male; F, female. **I.** Bar graphs showing chimerism of CD4$^+$ (left) and CD11b$^+$ (right) cells in the spleens of transplanted mice. Data are represented as mean±SD (n=9, from 3 independent experiments). Statistical difference was assessed using a paired t test, **** $p<0.0001$. **J.** Bar graph showing ratio of Ahr$^{-/-}$ to WT frequencies of indicated cell types in spleen and epidermis of transplanted mice. Data are represented as mean±SD (n=6 for epidermis and 9 for spleen, from 2 or 3 independent experiments). Significance was differences was assessed using a one-way ANOVA with Tukey's multiple comparisons test.

naling was sufficient to program mLCs that expressed both LC-defining transcription factors (*Id2*, *Ahr*) and genes upregulated within the skin environment (*Epcam*, *Cd207*, *Cldn1*, *Mfge8*) (Figure 6F). Moreover, direct comparison of our scRNA-seq gene signatures defining *in vivo* epidermal cell populations within our bulk RNA-seq dataset demonstrated that Jag1 signaling prescribed resident mLC identity (Figure 6G). The additional activation of Ahr signaling pushed cells towards a cycling mLC phenotype (Figure 6G).

Thus, Notch signaling is sufficient to restrict the differentiation potential of monocyte-derived cells, directing them away from a default macrophage program towards a mLC fate

Post-natal maturation of eLCs in human skin induces expression of DC-like immune gene programs that mirror mLC development. Our data demonstrate that MDP-derived monocytes adopt a distinct pathway of differentiation in murine adult skin, characterized by loss of Zeb2, to become mLCs. We therefore questioned whether such a transition away from a classical macrophage identity occurred in humans. Post-natal maturation of intestinal macrophages has been linked to the acquisition of immune functions (Viola *et al.* 2023). We posited that a similar maturation process occurred in human skin after birth, and was linked to LC specification. To address this, we analyzed a unique collection of samples taken from newborn babies (<28 days), infants (1 month - 1 year) and children (2-15 years) (Figure 7A). As previously demonstrated in mice and humans, we observed a marked expansion in eLC numbers in the transition from newborns to infants (Figure 7B). Bulk RNA-seq of sorted CD1a$^+$CD207$^+$ LCs further indicated that

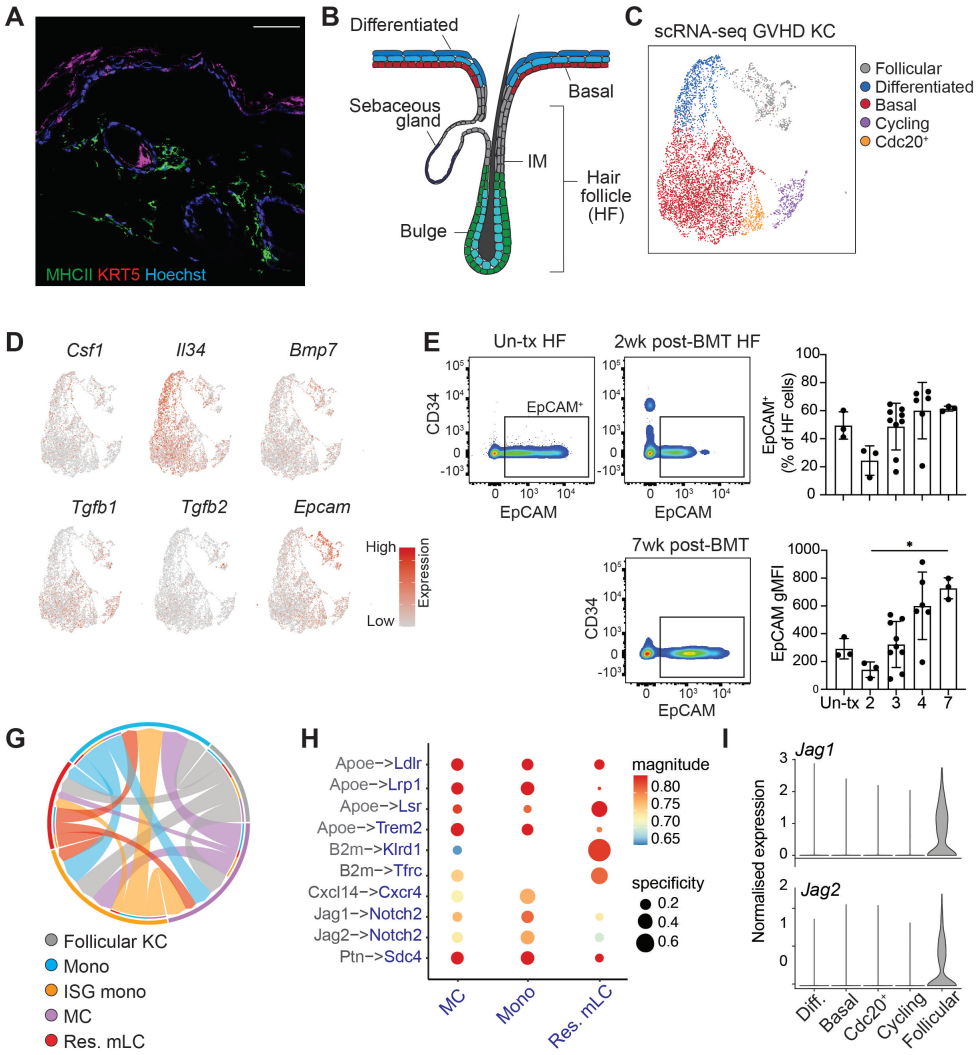

Fig. 5. A specialized keratinocyte niche permits mLC differentiation. **A.** Representative immunofluorescence staining of murine epidermis showing MHCII^{+} (green) cells clustering around KRT5^{+} hair follicle cells (red). Hoechst 33342 (blue) was used for nuclear staining. Scale bar = 50µm. **B.** Schematic representation of hair follicle structure found in the murine epidermis. IM, isthmus. **C.** UMAP visualisation and clustering of keratinocytes from the GVHD analysed by scRNA-seq. KC, keratinocytes **D.** Heatmap overlays showing normalized expression of indicated genes overlaid onto UMAP from (B). **E.** Representative flow plots showing EpCAM expression on hair follicle cells from untransplanted (Un-tx) and BMT + T epidermis. Gated on live, singlets, CD45^{neg}, Sca1^{neg} cells. **F.** Bar graphs showing quantification (above) and gMFI of EpCAM (below)from population indicated in (E). Data are represented as mean±SD (n=3 for control, n=3 for 2 weeks, 9 for 3 weeks, 7 for 4 weeks, 3 for 7 weeks). Data are pooled from three independent experiments. Significance was calculated using a Kruskal-Wallis test for multiple comparisons, p*<0.05. **G.** Chord plot showing potential receptor-ligand interactions between follicular KC (grey) and mono (blue), ISG Mono (orange), MC (purple) and res. mLC (red) assessed by LIANA. The width/weight of each arrow indicates the number of potential interactions identified. **H.** Dot plot showing specific interactions between follicular keratinocytes (grey) and indicated populations (blue). **I.** Violin plots showing normalized expression of indicated genes across scRNA-seq clusters.

this expansion was associated with a significant increase in transcriptional activity (Figure 7C). Visualization of the data as a co-expression network revealed a central gene program that is high in newborns and encodes basic macrophage functions including protein transport, RNA processing, and cadherin binding (Cluster 1,2, and 4, Figure 7D and Table S1). From this, other programs develop with age including processes of immune activation, including antigen processing and presentation, regulation of immune processes and regulation of response to external stimulus (Figures 7D, E and Table S1), suggesting that more DC-like functions were activated once the skin environment and LC network has fully matured. To determine how post-natal maturation of eLCs in human skin compared to mLC differentiation in adult murine skin we analyzed expression of the key factors associated with mLC development. Proliferation of eLCs in infant skin resulted in a marked loss of ZEB2 expression with concomitant up regulation of EPCAM, AHR and AHRR (Figure 7F).

In summary, we demonstrate that monocytes recruited to the epidermis after immune pathology adopt a unique pathway of differentiation to mLCs that mirrors post-natal program in human skin.

Discussion

Whether LCs are macrophages or DCs has long been debated (Lutz *et al.* 2017) and both denominations are still routinely applied in the literature, despite fate mapping studies demonstrating the embryonic macrophage origin for these cells (Ginhoux *et al.* 2006; Hoeffel *et al.* 2012; Schulz *et al.* 2012; Mass *et al.* 2016). Here we have begun to resolve this discussion demonstrating a selective bias in the cells that replenish the LC network after destruction of eLCs, whereby MDP-derived monocytes are more likely to become mLCs. Within the skin, localization and signaling within a unique hair follicle niche drives loss of the Zeb2, the regulator of tissue-resident macrophage identity at other barrier sites, and Notch-dependent expression of the LC-defining transcription factors Id2 and Ahr, to generate long-lived mLCs (Chopin *et al.* 2013; Mass *et al.* 2016). This adaptation to adult skin mirrors post-natal maturation of eLCs which is characterized by the appearance of a specific gene program associated with DC-like immune functions. Thus, specification of LCs within the skin environment drives evolution of a unique population of tissue-resident macrophages, which are the only resident macrophages that can migrate to draining lymph nodes and

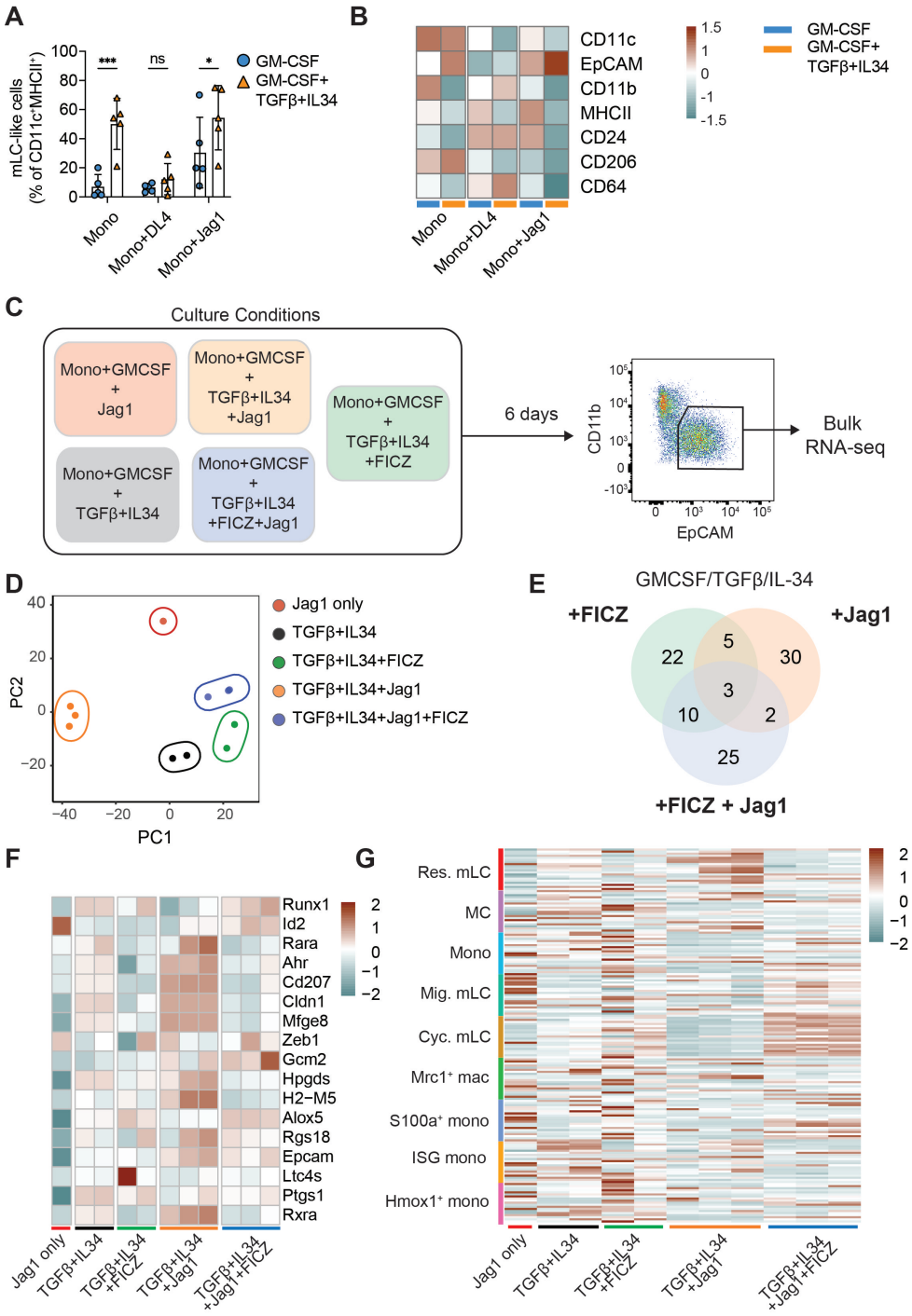

Fig. 6. Notch signaling programs mLC differentiation. A. Bar graph showing the proportion of mLC-like cells generated from monocytes cultured with GM-CSF alone or GM-CSF, TGFβ and IL34 in the presence or absence of indicated Notch ligands (see figure S6A for gating strategy). Data is shown as mean±SD (n=5). Significance was calculated by 2 way ANOVA with uncorrected Fisher's LSD for multiple comparisons, * $p<0.05$; ***$p<0.001$. **B.** Heatmap showing average gMFI of indicated markers from bone-marrow derived monocytes cultured and analysed by flow cytometry as indicated in (A) (n=5). **C.** Experimental set up for bulk RNA-seq of mLC-like cells generated under indicated conditions. **D.** PCA plot of bulk RNA-seq samples coloured by culture condition. **E.** Venn diagram showing numbers of common and unique DEGs between indicated conditions. **F.** Heatmap showing scaled expression of LC signature genes across samples. **G.** Heatmap showing expression of gene signatures from epidermal myeloid cell clusters (defined as top 20 DEGs) (y-axis) across bulk RNA-seq samples (x-axis).

prime T cell immunity.

We have exploited a murine model of skin immune pathology and eLC destruction to define the cellular and molecular pathways by which monocytes repair the LC network *in vivo*. ScRNA-seq of epidermal CD11b$^+$MHCII$^+$ cells revealed an unexpected heterogeneity wherein some monocytes appeared to undergo abortive default differentiation to CD206$^+$ macrophages whilst others received the required signals to direct them along the route towards a mLC fate. Metabolic analysis of differentiating cells suggests that macrophages fail to adopt pathways of fatty acid oxidation required for survival in the epidermis (Wculek *et al.* 2023). Moreover, whilst mLCs require IL-34 for their survival, CD206$^+$ macrophages may not receive CSF1 within the epidermis (Wang *et al.* 2012).

There is a growing awareness of the heterogeneity within Ly6C$^+$ monocytes, that represent a pool of cells derived from either GMPs or MDPs (Yáñez *et al.* 2017; Kwok *et al.* 2020; Trzebanski *et al.* 2023). We have recently identified phenotypic markers of GMP-Mos or MDP-Mos and combined this with fate mapping studies to define the contribution of these populations to tissue-resident macrophages; whilst both pop-

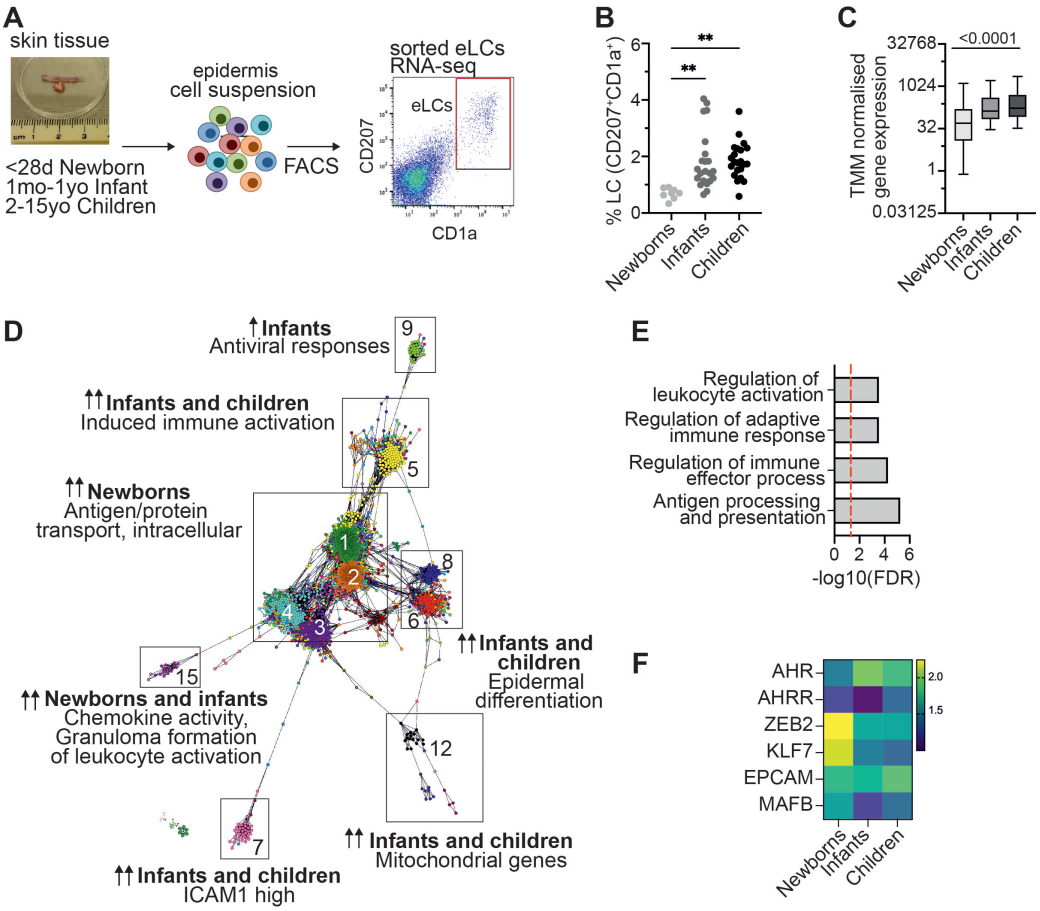

Fig. 7. Post-natal maturation of eLCs in human skin induces expression of DC-like immune gene programs that mirror mLC development. **A.** Human LCs isolation workflow. Skin from healthy donors aged 0-15 yo was digested with dispase at 4℃ overnight to separate epidermis from dermis. Epidermal cell suspension was obtained after 1.5h of liberase digestion of the epidermal sheet at 37℃. CD207$^+$CD1a$^+$ cells were FACS purified directly into Trizol. d, days; mo, months; yo, years old. **B.** Percentage of CD207$^+$CD1a$^+$ cells across newborns, infants and children. Significance was calculated by one way ANOVA, **p<0.01. **C.** Average TMM normalized gene expression levels in cluster 5 across newborns, infants and children. Significance was calculating using one way ANOVA. **D.** Transcript to transcript clustering Graphia, 2447 genes, r=0.75, MCL=1.7 identified 21 clusters with n>10 genes, encoding distinct transcriptional programs in human LCs. Arrows indicate enrichment. **E.** Gene ontology ranked with FDR corrected p-values given for cluster 5. **F.** Heatmap showing normalized expression of selected transcription factors.

ulations contributed equally to different gut macrophage populations, different lung interstitial macrophage populations were derived from GMPs or DCMos (Trzebanski *et al.* 2023). Here we show that, despite the relative scarcity of MDP compared to GMP in BM, MDP-Mos selectively accumulate in the epidermis to become mLCs. MDPs, but not GMPs gave rise to CD11b^{low}EpCAM$^+$ mLCs *in vitro*, suggesting intrinsic bias towards responsiveness to epidermal growth factors. Further experiments are needed to test whether the relative abundance of MDP-Mos in the epidermis is due selective recruitment and entry of DCMo and/or preferential expansion and survival of these cells and their progeny within the epidermal niche.

Ahr is an evolutionarily conserved cytosolic sensor that functions as a ligand-dependent transcription factor to control cell fate decisions in gut immune cells (Stockinger, 2009), and direct monocytes towards a DC-like rather than a macrophage endpoint (Goudot *et al.* 2017). The role of Ahr signaling in LCs remains unclear; eLC begin to express Ahr upon differentiation *in utero* (Mass *et al.* 2016), but our data suggest that expression increases post-birth. The epidermis of Ahr-deficient mice is replete with LCs (Esser, Rannug and Stockinger, 2009), albeit, a less activated population, probably due to the absence of dendritic epidermal T cells (DETC) and reduced GM-CSF production in the skin of these mice (Jux, Kadow and Esser, 2009). Moreover, mice fed with chow deficient in Ahr dietary ligands had normal numbers of LCs (Cros *et al.* 2023), but these cells did not migrate to draining LNs. In contrast, in one study, LC-specific deletion of Ahr led to a reduction in epidermal LCs (Hong *et al.* 2020). We tested the role of Ahr signaling for the differentiation of mLCs and found that blockade of Ahr prevented monocyte differentiation *in vitro*, supporting a previous study using CD34$^+$ precursors (Platzer *et al.* 2009). However, use of competitive chimeras demonstrated that Ahr-deficient monocytes could become mLCs *in vivo*. We observed that canonical (Cyp1b1) Ahr signaling was active in mLCs *in vitro* but not *in vivo* suggesting activation of alternative pathways within the epidermal environment.

To determine the extrinsic signals regulating mLC development we characterized the epidermal niche and identified a spatially restricted area of the follicular epidermis at which homotypic binding of EpCAM$^+$ MCs provides access to local Notch signals. Monocytes are recruited to the epidermis via CCL2-secreting isthmus epithelial cells before migration to the inter follicular epidermis (Nagao *et al.* 2012), where they are retained due to localized activation of latent TGFβ by αvβ6 integrins (Mohammed *et al.* 2016). Our data demonstrate that the follicular niche is not only a site of recruitment but also provides instructive signals for differentiation to mLCs before they relocate within the keratinocytes of the differentiated epidermis. Notch signaling with TGFβ promotes human moLC development *in vitro* (Strobl, Krump and Borek, 2019; Bellmann *et al.* 2021). A recent study that

employed scRNA-seq of human LCs revealed the presence of 2 eLC populations in the skin, linking Notch signaling to expansion of EpCAM^{neg} cells (Liu *et al.* 2021). By contrast, our data suggest that Notch signaling restricts murine monocyte differentiation to becoming mLCs at the expense of other fates. It is possible that Notch signaling promotes a more DC-like program in mLCs; Notch signaling in monocytes has been shown to suppress a macrophage fate in favor of a DC fate and is required for differentiation to monocyte-derived CD207^{+}CD1a^{+} cells characteristic of LC histiocytosis (Kvedaraite *et al.* 2022).

Inflammation due to UV irradiation or GVHD leads to influx of wave(s) of monocytes, the majority of which will not succeed in becoming long-lived LCs (Ginhoux *et al.* 2006; Seré *et al.* 2012). We previously used mathematical modelling to define the cellular processes by which monocytes refill the empty epidermis, demonstrating a significant inefficiency whereby only 4% of epidermal monocytes were predicted to become long-lived mLCs (Ferrer *et al.* 2019). Our data now explain this inefficiency by demonstrating: first, that only a subset of Ly6C^{+} monocytes can become mLCs; and second, that LC precursors compete for Notch signals within a spatially restricted hair follicle niche.

Evidence for the macrophage-origin of embyronic LCs comes from reporter studies in which labelled yolk sac (Schulz *[et al.* 2012; Mass *et al.* 2016) and fetal liver (Hoeffel *et al.*, 2012) macrophage/monocytes gave rise to the nascent LC network in the developing embryo. Moreover, use of the macrophage-restricting gene MafB to lineage trace myeloid cells labelled all LCs in the healthy adult skin (Wu *et al.*, 2016), and generation of LCs from CD34^{+} stem cells requires suppression of the transcription factor Klf4, which is associated with differentiation of moDCs (Jurkin *et al.*, 2017). But, LCs express high levels of CD24 and Zbtb46, considered markers of conventional DCs (Wu *et al.*, 2016), more activation and migration initiates the expression of convergent transcriptional program shared with DC populations leaving the skin (Clayton *et al.*, 2017; Polak and Singh, 2021; Reynolds *et al.*, 2021). Migrating LCs upregulate an IRF4-dependent gene program which is also evident in moDC (Sirvent *et al.*, 2020; Davies *et al.*, 2022). We believe our data begin to reconcile this dichotomy. Zeb2 is a critical regulator of cell fate that specifies tissue-resident macrophage identity across barrier sites (Scott *et al.*, 2018; Anderson *et al.*, 2021) and we show that only those cells that have lost Zeb2 expression upregulate EpCAM to become mLCs. Key regulatory elements control function in embryonic and HSC-derived macrophages, of which Zeb2^{-165} is utilized by HSCs and regulates mutual exclusivity with Id2 expression (Huang *et al.*, 2021). This molecular cross-talk has been shown to determine cDC2 specification (Liu *et al.*, 2022) and we speculate that a similar process may permit expression of Id2 in differentiating mLCs, and initiating the shift from more macrophage-like to DC-like cells.

Murine and human eLCs undergo a burst of proliferation after birth (Chorro *et al.*, 2009; Meindl *et al.*, 2009), but it was not known whether expansion of eLC was associated with maturation of the network, as has been demonstrated for the LCs of the oral mucosa (Jaber *et al.*, 2023). To address this question, we assembled a unique RNA-seq dataset from eLCs sorted from newborn children, up to 1 year-old infants and older children. These data revealed the documented increase in LC density after the first 28 days of life (Meindl *et al.*, 2009) and demonstrated that this increase was associated with a marked change in gene expression whereby the macrophage-associated genes MAFB and ZEB2 were downregulated, while we observed an increase in AHR and EPCAM. Notably, this transition was accompanied by the expression of gene modules associated with enhanced immune and DC-like functions. These findings support our proposed concept of gene regulatory networks defining LC function whereby interaction between Ahr and Irf4 activates expression of immunogenic function and migration to LNs (Polak and Singh, 2021). The signals that trigger eLC proliferation in the skin are not known, but an attractive hypothesis is that this is due to interactions with microbiota. Whilst skin commensal bacteria per se are not required for LC development and survival (Capucha *et al.*, 2018), it is possible that the increase in microbiota diversity during the first year of life could play an important role in conditioning the LC niche. Further experiments are required to test this hypothesis.

In conclusion, we suggest that the LC functional dichotomy may reflect a changing requirement throughout development; whilst integral macrophage-biased tissue repair functions may be required for skin organogenesis, a distinct more immune-biased role maintaining the skin immune barrier may become more important in adult skin, and this is imprinted after birth. This concept is supported by the detailed analysis of developing skin demonstrating that embryonic gene programs are overlaid with maturation, but cells may revert back to these programs under diseased conditions (Reynolds *et al.*, 2021). Convergent evolution of monocytes within adult skin permits expression of these gene programs to generate a population of LCs to replenish the epidermal niche.

Materials and methods

Mice. C57BL/6 (B6) were purchased from Charles River UK. Langerin.DTR^{GFP} were originally provided by Adrian Kissenpfennig and Bernard Malissen (Kissenpfennig *et al.*, 2005), T cell receptor (TCR)-transgenic anti-HY Matahari were provided by Jian Chai (Imperial College London, London, UK)(Valujskikh *et al.*, 2002) and CD45.1 mice were bred in-house at University College London (UCL) Biological Services Unit. ID2^{BFP} reporter mice were a kind gift from Andrew McKenzie (University of Cambridge), whereby the pBAD-mTagBFP2 plasmid was a gift from Vladislav Verkhusha (Addgene plasmid no. 34632 ; http://n2t.net/addgene:34632 ; RRID:Addgene_34632) (Subach *et al.*, 2011; Walker *et al.*, 2019). All procedures were conducted in accordance with the UK Home Office Animals (Scientific Procedures) Act of 1986 and were approved by the Ethics and Welfare Committee of the Comparative Biol-

ogy Unit (Hampstead Campus, UCL, London, UK).

Human samples. Human skin samples were collected with written informed consent from donors with approval by the South East Coast - Brighton & Sussex Research Ethics Committee in adherence to Helsinki Guidelines [ethical approvals: REC approval: 16/LO/0999).

Bone marrow transplants. Recipient male CD45.2 B6 mice were lethally irradiated (10.4Gy of total body irradiation, split into two fractions sepatated by 48 hours) and reconstituted 4 hours after the second dose with 5 x 10^6 female CD45.1 B6 bone marrow (BM) cells, 2 x 10^6 CD4 T cells, with 1 x 10^6 CD8 Matahari T cells administered by intravenous injection through the tail vein. CD4 and CD8 donor T cells were isolated from spleen and lymph node single cell suspensions by magnetic activation cell sorting (MACS; Miltenyi) using CD4 (L3T4) and CD8a (Ly-2) microbeads (Miltenyi) according to manufacturer's instructions. In some experiments, BM from $ID2^{BFP}$ B6 mice was used to track donor LC. In some experiments, $Langerin.DTR^{GFP}$ male mice were used as recipients to track host LCs.

Mixed chimera experiments. BM from $AHR^{-/-}$ mice was a gift from Brigitta Stockinger (Francis Crick Institute) (Schmidt *et al.*, 1996). Lethally irradiated male $Langerin.DTR^{GFP}$ B6 mice received a 50:50 mix of BM from $AHR^{-/-}$ and $ID2^{BFP}$ female mice, with CD4 T cells and CD8 Matahari T cells. Three weeks following transplant, epidermis and spleens were processed and analysed for chimerism by flow cytometry.

Tissue processing. Murine skin: Epidermal single cell suspensions were generated as described (Ferrer *et al.*, 2019; West *et al.*, 2022). Dorsal and ventral sides of the ear pinna were split using forceps. These were floated on Dispase II (2.5mg/ml; Roche), in HBSS and 2% FCS for 1 hour at 37°C or overnight at 4°C, followed by mechanical dissociation of the epidermal layer by mincing with scalpels. Cells were passed sequentially through 70- and 40µm cell strainers in 1mM EDTA, 1% FCS, PBS solution. **Human skin:** Fat and lower dermis was cut away and discarded before dispase (2 U/ml, Gibco, UK) digestion for 20h at 4°C. Epidermal sheets were digested in Liberase™ (13 U/ml, Roche, UK), for 1.5h at 37°C. **Bone marrow:** Bone marrow single cell suspensions were prepared from femurs and tibias of donors using a mortar and pestle. Red blood cells were lysed in 1ml of ammonium chloride (ACK buffer) for 1 min at room temperature. Cells were washed and resuspended in complete RPMI (RPMI supplemented with 10% FCS, 1% L-glutamine, 1% Penicillin-streptomycin) until used.

***In vitro* cultures. GMP and MDP cultures:** GMP, MDP and $Ly6C^{hi}$ monocytes from whole bone marrow were FACS isolated and up to $2x10^3$ cells were seeded in 96-well flat-bottom tissue-culture treated plates. Cells were cultured in complete RPMI and supplemented with with recombinant GM-CSF (20ng/ml; Peprotech), TGFβ (5ng/ml; R&D systems) and IL34 (8µg/ml; R&D systems). Cells were cultured at 37°C, 5% CO_2. The medium was partially replaced on day 2 of culture and completely replaced on day 3, and cells were harvested on day 6. **Monocyte cultures:** Monocytes were isolated from whole bone marrow by MACS using Monocyte Isolation Kit (BM; Miltenyi, 130-100-629) as per manufacturer's instructions. Monocytes were resuspended in complete RPMI and plated at $5x10^5$ cells per well in tissue-culture treated 24-well plates. Cells were cultured as described above. **Monocyte-OP9 co-cultures:** OP9, OP9-Jag1 and OP9-DL4 cell lines were gifted by Victor Tybulewicz (Francis Crick Institute) and were cultured in RPMI supplemented with 10% FCS, 1% L-glutamine, 1% Penicillin-streptomycin, MEM NEAA, sodium pyruvate, HEPES buffer and ß-mercaptoethanol. OP9 cells were seeded onto tissue-culture treated 24-well plates at 2 x 10^4 cells per well and incubated overnight at 37°C. The next day, following monocyte isolation, cells were counted, and 1 x 10^5 monocytes were seeded on to OP9 cells. Cells were cultured as described above.

Flow cytometry and cell sorting. Murine: Cells were distributed into 96-well V-bottom plates or FACS tubes and incubated in 2.4G2 hybridoma supernatant for 10 min at 4°C to block Fc receptors. Cells were washed with FACS buffer (2% FCS, 2mM EDTA, PBS) before adding antibody cocktails that were prepared in a total volume of 50µl per test in Brilliant Stain Buffer (BD Biosciences) and FACS buffer. Cells were incubated with antibodies for 30 mins on ice then washed with FACS buffer. Viability was assessed either by staining cells with Fixable Viability Dye eFluor680 (eBiosciences) or Propidium iodide (PI), for fixed or unfixed cells respectively. For intracellular staining, cells were fixed and permeabilized using the Foxp3/Transcription Factor Staining Buffer Set (Invitrogen) for 30 mins on ice. Cells were subsequently washed in permeabilization buffer before adding antibody cocktails that were prepared in a total volume of 50µl per test in permeabilization buffer. Cells were incubated with antibodies for 30 mins on ice then washed with permeabilization buffer. Antibodies used are listed in table S2. **Human:** Antibodies used for cell staining were pre-titrated and used at optimal concentrations. For FACS purification LCs were stained for CD207 (anti-CD207 PeVio700), CD1a (anti-CD1a VioBlue) and HLA-DR (anti-HLA-DR Viogreen, Miltenyi Biotech, UK).

When required, cells were acquired on a BD Fortessa analzyer equipt with BD FACSDiva software; or sorted into either complete RPMI or RLT lysis buffer (Qiagen) or Trizol using a BD Aria III.

Single cell RNA-sequencing. Single cell suspensions from murine epidermis were stained for FACS as described above. Donor and host $CD11b^+MHCII^+$ cells as well as $CD45^{neg}$ cells were sorted into RPMI medium supplemented 2% FCS and counted manually. Cell concentrations were adjusted to 500-1200 cells/µl and loaded at 7,000-15,000 cells per chip position using the 10X Chromium Single cell 5' Library, Gel

Bead and Multiplex Kit and Chip Kit (10X Genomics, V3 barcoding chemistry) according to manufacturer's instructions. Data are from multiple mice sorted from 2 independent BMT experiments. All subsequent steps were performed following standard manufacturer's instructions. Purified libraries were analysed by an Illumina Hiseq X Ten sequencer with 150-bp paired-end reads. ***scRNA-seq data processing and analyses.*** Generated scRNA-seq data were preprocessed using the kallisto and bustools workflow (Melsted *et al.*, 2021). Downstream analysis was performed using the Seurat package in R (Stuart *et al.*, 2019). Cells with <500 detected genes and >20% mitochondrial gene expression were removed from the dataset. DoubletFinder was used to identify and remove any likely doublets. These were typically less than 1% of each batch. PCA was performed on the 2000 most variable genes and clusters were identified using the Leiden algorithm. Clusters were annotated based on the expression of key cell-type defining genes. Differentially expressed genes (DEGs) were identified using the FindMarkers function with significance cut offs of log2-fold change > 2 and adjusted p-values < 0.05. ***Enrichment score analysis.*** To calculate enrichment scores for specific gene signatures the Seurat function AddModuleScore was used. The human migLC gene signature included 101 genes (Sirvent *et al.*, 2020). The MDP-Mo and GMP-Mo signatures included 140 and 108 genes respectively (Trzebanski *et al.*, 2023). ***Trajectory analyses.*** Pseudotime trajectory inference of differentiation was performed using the Slingshot and RNA velocity packages for R (La Manno *et al.*, 2018). Differential expression testing of genes along and between different branches of these trajectories were identified by tradeseq velocity analysis using the velociraptor package, which infers directionality of differentiation. ***Receptor-ligand interaction analysis.*** Potential receptor-ligand (R-L) interactions between the follicular keratinocyte subset and monocyte-derived cell clusters were investigated using the LIANA package (Dimitrov *et al.*, 2022). LIANA is an umbrella framework which creates a consensus R-L score from the methods and pathway tools of several other software packages. It encompasses CellPhoneDB (v2), CellChat, NATMI, iTALK and CytoTalk (Dimitrov *et al.*, 2022). ***SCENIC analysis.*** SCENIC was used to identify regulons, sets of transcription factors and their cofactors co-expressed with their downstream targets in single cell data (Aibar *et al.*, 2017). This analysis was applied to the 10X scRNA-seq dataset and each of the regulon AUC per cell scores was used to identify regulons with the greatest mean difference between Res-mLC and all other clusters. ***COMPASS analysis.*** *In silico* flux balance analysis was conducted via COMPASS (Wagner *et al.*, 2021). Normalized scRNA-seq counts per million (CPM) gene expression profiles were exported and COMPASS analysis was conducted using standard settings on a high-performance computing cluster (Butcher, King and Zalewski, 2017). Metabolic reactions were mapped to RECON2 reaction metadata (Thiele *et al.*, 2013), and reaction activity scores were calculated from reaction penalties. Reactions which do not have an enzyme commission number or for which there is no biochemical support (RECON2 confidence score = 1-3) were excluded from the analysis. Differential reaction activities were analysed via Wilcoxon rank-sum testing and resulting p-values were adjusted via the Benjamini-Hochberg (BH) method. Reactions with an adjusted p-value of less than 0.1 were considered differentially active. Effect sizes were assessed with Cohen's d statistic.

Bulk RNA-seq and analyses. Up to $1x10^5$ cells were FACS sorted directly into RLT lysis buffer (Qiagen) supplemented with 14mM β-mercaptoethanol. Cells were vortexed immediately after being sorted to ensure cell lysis. RNA was extracted using the RNeasy Micro kit (Qiagen) as per manufacturer's instructions, with an additional DNA clean-up step using RNase-free DNase I (Qiagen). RNA quantification and quality check was carried out by Novogene (UK), as well as subsequent library preparation and sequencing. Sequencing was performed on a NovaSeq 600 System (Illumina) to yield an average of 30 million reads per sample.

RNA-seq transcript abundance was quantified using the salmon read mapper and an Ensembl GRCm39 transcript model. The data were imported to the R statistical environment and summarized at the gene level (that is, transcript counts summed) using tximport. Statistical transformations for visualisation (vst and log10) and analyses of differential expression were performed using the DESeq2 package (Love, Huber and Anders, 2014). Multiple testing adjustments of differential expression utilized the Benjamini–Hochberg false discovery rate (fdr).

RT-PCR. RNA was extracted from samples as described above. RNA quantification was carried out using a Nanodrop and cDNA was synthesized using the High-Capacity cDNA Reverse Transcription Kit (Applied Biosystems) as per manufacturer's instructions. RT-PCR was run on a QuantStudio 5 Real-Time PCR system (Thermo Fisher Scientific) using the Maxima SYBR Green/ROX qPCR Master Mix (2X) (Thermo Fisher Scientific) according to manufacturer's instructions. Primers used in this study: *Ahr* forward, AGC CGG TGC AGA AAA CAG TAA; *Ahr* reverse, AGG CGG TCT AAC TCT GTG TTC; *Cyp1b1* forward, ACG ACG ATG CGG AGT TCC TA; *Cyp1b1* reverse, CGG GTT GGG AAA TAG CTG C; *GAPDH* forward, CGGGTTCCTATAAATACGGACTGC; *GAPDH* reverse, GTTCACACCGACCTTCACCA.

Immunofluorescence imaging. Skin biopsies were embedded in OCT compound (Leica). 10 mm sections were cut using a cryostat (Leica) and stored at -20°C. Tissue was blocked for 2 hours at room temperature with 5% BSA (Sigma Aldrich), 5% Donkey Serum (Merck) in 0.01% PBS-Tween-20 (PBST). Sections were incubated with primary antibodies for KRT5 (Covance; PRB-160P) and MHCII (Abcam; ab15630) overnight at 4°C. Antibodies were detected using donkey Cy2- or Cy5-conjugated secondary Fab fragment antibodies (Jackson Laboratories) and nuclei stained using Hoechst 33342 (1:1000, Sigma Aldrich), and mounted using Prolong Gold anti-fade mounting media. Images were

acquired on a Leica SP8 confocal microscope and subsequently analyzed using NIH ImageJ software.

Statistical analyses. All data, apart from RNA-seq data, were analyzed using GraphPad Prism Version 6.00 for Mac OsX (GraphPad Software, USA). All line graphs and bar charts are shown as mean±SD. Protein expression data for flow cytometry is shown as geometric mean fluorescent intensity (as specified in figure legends) with the range. Significant differences were determined using one-way analysis of variance (ANOVA) to measure a single variable in three groups or two-way ANOVA for experiments with more than one variable, with post-tests specified in individual figure legends. For comparisons between 2 paired groups a paired t test was used according to a normality test. Significance was defined as *$p < 0.05$, **$p < 0.01$, ***$p < 0.001$, ****$p <$. 0.0001. Statistical details of the data can be found in each figure legend. Analysis of bulk and scRNA-seq data was performed in the R and Python environments using tests described in the method details.

References

Aibar, S., González-Blas, C.B., Moerman, T., Huynh-Thu, V.A., Imrichova, H., Hulselmans, G., Rambow, F., Marine, J.-C., Geurts, P., Aerts, J., van den Oord, J., Atak, Z.K., Wouters, J., Aerts, S., 2017. SCENIC: single-cell regulatory network inference and clustering. Nat. Methods 14, 1083–1086. https://doi.org/10.1038/nmeth.4463

Anderson, D.A., Dutertre, C.-A., Ginhoux, F., Murphy, K.M., 2021. Genetic models of human and mouse dendritic cell development and function. Nat. Rev. Immunol. 21, 101–115. https://doi.org/10.1038/s41577-020-00413-x

Baratin, M., Foray, C., Demaria, O., Habbeddine, M., Pollet, E., Maurizio, J., Verthuy, C., Davanture, S., Azukizawa, H., Flores-Langarica, A., Dalod, M., Lawrence, T., 2015. Homeostatic NF-κB Signaling in Steady-State Migratory Dendritic Cells Regulates Immune Homeostasis and Tolerance. Immunity 42, 627–639. https://doi.org/10.1016/j.immuni.2015.03.003

Bellmann, L., Zelle-Rieser, C., Milne, P., Resteu, A., Tripp, C.H., Hermann-Kleiter, N., Zaderer, V., Wilflingseder, D., Hörtnagl, P., Theochari, M., Schulze, J., Rentzsch, M., Del Frari, B., Collin, M., Rademacher, C., Romani, N., Stoitzner, P., 2021. Notch-Mediated Generation of Monocyte-Derived Langerhans Cells: Phenotype and Function. J. Invest. Dermatol. 141, 84-94.e6. https://doi.org/10.1016/j.jid.2020.05.098

Bennett, C.L., Perona-Wright, G., 2023. Metabolic adaption of mucosal macrophages: Is metabolism a driver of persistence across tissues? Mucosal Immunol. 16, 753–763. https://doi.org/10.1016/j.mucimm.2023.06.006

Bommer, G.T., MacDougald, O.A., 2011. Regulation of Lipid Homeostasis by the Bifunctional SREBF2-miR33a Locus. Cell Metab. 13, 241–247. https://doi.org/10.1016/j.cmet.2011.02.004

Bonnardel, J., T'Jonck, W., Gaublomme, D., Browaeys, R., Scott, C.L., Martens, L., Vanneste, B., Prijck, S.D., Nedospasov, S.A., Kremer, A., Hamme, E.V., Borghgraef, P., Toussaint, W., Bleser, P.D., Mannaerts, I., Beschin, A., Grunsven, L.A. van, Lambrecht, B.N., Taghon, T., Lippens, S., Elewaut, D., Saeys, Y., Guilliams, M., 2019. Stellate Cells, Hepatocytes, and Endothelial Cells Imprint the Kupffer Cell Identity on Monocytes Colonizing the Liver Macrophage Niche. Immunity 51, 638-654.e9. https://doi.org/10.1016/j.immuni.2019.08.017

Butcher, S., King, T., Zalewski, L., 2017. Apocrita - High Performance Computing Cluster for Queen Mary University of London. https://doi.org/10.5281/zenodo.438045

Capucha, T., Koren, N., Nassar, M., Heyman, O., Nir, T., Levy, M., Zilberman-Schapira, G., Zelentova, K., Eli-Berchoer, L., Zenke, M., Hieronymus, T., Wilensky, A., Bercovier, H., Elinav, E., Clausen, B.E., Hovav, A.-H., 2018. Sequential BMP7/TGF-β1 signaling and microbiota instruct mucosal Langerhans cell differentiation. J. Exp. Med. 215, 481–500. https://doi.org/10.1084/jem.20171508

Chopin, M., Seillet, C., Chevrier, S., Wu, L., Wang, H., Morse, H.C., Belz, G.T., Nutt, S.L., 2013. Langerhans cells are generated by two distinct PU.1-dependent transcriptional networks. J. Exp. Med. 210, 2967–2980. https://doi.org/10.1084/jem.20130930

Chorro, L., Sarde, A., Li, M., Woollard, K.J., Chambon, P., Malissen, B., Kissenpfennig, A., Barbaroux, J.-B., Groves, R., Geissmann, F., 2009. Langerhans cell (LC) proliferation mediates neonatal development, homeostasis, and inflammation-associated expansion of the epidermal LC network. J. Exp. Med. 206, 3089–3100. https://doi.org/10.1084/jem.20091586

Clayton, K., Vallejo, A.F., Davies, J., Sirvent, S., Polak, M.E., 2017. Langerhans Cells—Programmed by the Epidermis. Front. Immunol. 8, 1676. https://doi.org/10.3389/fimmu.2017.01676

Collin, M.P., Hart, D.N.J., Jackson, G.H., Cook, G., Cavet, J., Mackinnon, S., Middleton, P.G., Dickinson, A.M., 2006. The fate of human Langerhans cells in hematopoietic stem cell transplantation. J. Exp. Med. 203, 27–33. https://doi.org/10.1084/jem.20051787

Cros, A., De Juan, A., Leclère, R., Sampaio, J.L., San Roman, M., Maurin, M., Heurtebise-Chrétien, S., Segura, E., 2023. Homeostatic activation of aryl hydrocarbon receptor by dietary ligands dampens cutaneous allergic responses by controlling Langerhans cells migration. eLife 12, e86413. https://doi.org/10.7554/eLife.86413

Dimitrov, D., Türei, D., Garrido-Rodriguez, M., Burmedi, P.L., Nagai, J.S., Boys, C., Ramirez Flores, R.O., Kim, H., Szalai, B., Costa, I.G., Valdeolivas, A., Dugourd, A., Saez-Rodriguez, J., 2022. Comparison of methods and resources for cell-cell communication inference from single-cell RNA-Seq data. Nat. Commun. 13, 3224. https://doi.org/10.1038/s41467-022-30755-0

Elbe-Bürger, A., Schuster, C., 2010. Development of the prenatal cutaneous antigen-presenting cell network. Immunol. Cell Biol. 88, 393–399. https://doi.org/10.1038/icb.2010.13

Esser, C., Rannug, A., Stockinger, B., 2009. The aryl hydrocarbon receptor in immunity. Trends Immunol. 30, 447–454. https://doi.org/10.1016/j.it.2009.06.005

Ferrer, I.R., West, H.C., Henderson, S., Ushakov, D.S., Santos e Sousa, P., Strid, J., Chakraverty, R., Yates, A.J., Bennett, C.L., 2019. A wave of monocytes is recruited to replenish the long-term Langerhans cell network after immune injury. Sci. Immunol. 4, eaax8704. https://doi.org/10.1126/sciimmunol.aax8704

Finlay, C.M., Parkinson, J.E., Zhang, L., Chan, B.H.K., Ajendra, J., Chenery, A., Morrison, A., Kaymak, I., Houlder, E.L., Murtuza Baker, S., Dickie, B.R., Boon, L., Konkel, J.E., Hepworth, M.R., MacDonald, A.S., Randolph, G.J., Rückerl, D., Allen, J.E., 2023. T helper 2 cells control monocyte to tissue-resident macrophage differentiation during nematode infection of the pleural cavity. Immunity 56, 1064-1081.e10. https://doi.org/10.1016/j.immuni.2023.02.016

Ginhoux, F., Tacke, F., Angeli, V., Bogunovic, M., Loubeau, M., Dai, X.-M., Stanley, E.R., Randolph, G.J., Merad, M., 2006. Langerhans cells arise from monocytes in vivo. Nat. Immunol. 7, 265–273. https://doi.org/10.1038/ni1307

Goodman, W.A., Omenetti, S., Date, D., Di Martino, L., De Salvo, C., Kim, G.-D., Chowdhry, S., Bamias, G., Cominelli, F., Pizarro, T.T., Mahabeleshwar, G.H., 2016. KLF6 contributes to myeloid cell plasticity in the pathogenesis of intestinal inflammation. Mucosal Immunol. 9, 1250–1262. https://doi.org/10.1038/mi.2016.1

Gosselin, D., Link, V.M., Romanoski, C.E., Fonseca, G.J., Eichenfield, D.Z., Spann, N.J., Stender, J.D., Chun, H.B., Garner, H., Geissmann, F., Glass, C.K., 2014. Environment Drives Selection and Function of Enhancers Controlling Tissue-Specific Macrophage Identities. Cell 159, 1327–1340. https://doi.org/10.1016/j.cell.2014.11.023

Goudot, C., Coillard, A., Villani, A.-C., Gueguen, P., Cros, A., Sarkizova, S., Tang-Huau, T.-L., Bohec, M., Baulande, S., Hacohen, N., Amigorena, S., Segura, E., 2017. Aryl Hydrocarbon Receptor Controls Monocyte Differentiation into Dendritic Cells versus Macrophages. Immunity 47, 582-596.e6. https://doi.org/10.1016/j.immuni.2017.08.016

Grabski, I.N., Street, K., Irizarry, R.A., 2023. Significance analysis for clustering with single-cell RNA-sequencing data. Nat. Methods 20, 1196–1202. https://doi.org/10.1038/s41592-023-01933-9

Greter, M., Lelios, I., Pelczar, P., Hoeffel, G., Price, J., Leboeuf, M., Kündig, T.M., Frei, K., Ginhoux, F., Merad, M., Becher, B., 2012. Stroma-Derived Interleukin-34 Controls the Development and Maintenance of Langerhans Cells and the Maintenance of Microglia. Immunity 37, 1050–1060. https://doi.org/10.1016/j.immuni.2012.11.001

Hoeffel, G., Wang, Y., Greter, M., See, P., Teo, P., Malleret, B., Leboeuf, M., Low, D., Oller, G., Almeida, F., Choy, S.H.Y., Grisotto, M., Renia, L., Conway, S.J., Stanley, E.R., Chan, J.K.Y., Ng, L.G., Samokhvalov, I.M., Merad, M., Ginhoux, F., 2012. Adult Langerhans cells derive predominantly from embryonic fetal liver monocytes with a minor contribution of yolk sac–derived macrophages. J. Exp. Med. 209, 1167–1181. https://doi.org/10.1084/jem.20120340

Hong, C.-H., Lin, S.-H., Clausen, B.E., Lee, C.-H., 2020. Selective AhR knockout in langerin-expressing cells abates Langerhans cells and polarizes Th2/Tr1 in epicutaneous protein sensitization. Proc. Natl. Acad. Sci. 117, 12980–12990. https://doi.org/10.1073/pnas.1917479117

Huang, X., Ferris, S.T., Kim, S., Choudhary, M.N.K., Belk, J.A., Fan, C., Qi, Y., Sudan, R., Xia, Y., Desai, P., Chen, J., Ly, N., Shi, Q., Bagadia, P., Liu, T., Guilliams, M., Egawa, T., Colonna, M., Diamond, M.S., Murphy, T.L., Satpathy, A.T., Wang, T., Murphy, K.M., 2021. Differential usage of transcriptional repressor Zeb2 enhancers distinguishes adult and embryonic hematopoiesis. Immunity 54, 1417-1432.e7. https://doi.org/10.1016/j.immuni.2021.04.015

Jaber, Y., Netanely, Y., Naamneh, R., Saar, O., Zubeidat, K., Saba, Y., Georgiev, O., Kles, P., Barel, O., Horev, Y., Yosef, O., Eli-Berchoer, L., Nadler, C., Betser-Cohen, G., Shapiro, H., Elinav, E., Wilensky, A., Hovav, A.-H., 2023. Langerhans cells shape postnatal oral homeostasis in a mechanical-force-dependent but microbiota and IL17-independent manner. Nat. Commun. 14, 5628. https://doi.org/10.1038/s41467-023-41409-0

Jakob, T., Udey, M.C., 1999. Epidermal Langerhans cells: from neurons to nature's adjuvants. Adv. Dermatol. 14, 209–58. https://doi.org/PMID: 10643500

Joost, S., Zeisel, A., Jacob, T., Sun, X., La Manno, G., Lönnerberg, P., Linnarsson, S., Kasper, M., 2016. Single-Cell Transcriptomics Reveals that Differentiation and Spatial Signatures Shape Epidermal and Hair Follicle Heterogeneity. Cell Syst. 3, 221-237.e9. https://doi.org/10.1016/j.cels.2016.08.010

Joseph, J.V., Conroy, S., Pavlov, K., Sontakke, P., Tomar, T., Eggens-Meijer, E., Balasubramaniyan, V., Wagemakers, M., Den Dunnen, W.F.A., Kruyt, F.A.E., 2015. Hypoxia enhances migration and invasion in glioblastoma by promoting a mesenchymal shift mediated by the HIF1α–ZEB1 axis. Cancer Lett. 359, 107–116. https://doi.org/10.1016/j.canlet.2015.01.010

Jurkin, J., Krump, C., Köffel, R., Fieber, C., Schuster, C., Brunner, P.M., Borek, I., Eisenwort, G., Lim, C., Mages, J., Lang, R., Bauer, W., Mechtcheriakova, D., Meshcheryakova, A., Elbe-Bürger, A., Stingl, G., Strobl, H., 2017. Human skin dendritic cell fate is differentially regulated by the monocyte identity factor Kruppel-like factor 4 during steady state and inflammation. J. Allergy Clin. Immunol. 139, 1873-1884.e10. https://doi.org/10.1016/j.jaci.2016.09.018

Jux, B., Kadow, S., Esser, C., 2009. Langerhans Cell Maturation and Contact Hypersensitivity Are Impaired in Aryl Hydrocarbon Receptor-Null Mice. J. Immunol. 182, 6709–6717. https://doi.org/10.4049/jimmunol.0713344

Kaplan, D.H., 2017. Ontogeny and function of murine epidermal Langerhans cells. Nat. Immunol. 18, 1068–1075. https://doi.org/10.1038/ni.3815

Kissenpfennig, A., Henri, S., Dubois, B., Laplace-Builhé, C., Perrin, P., Romani, N., Tripp, C.H., Douillard, P., Leserman, L., Kaiserlian, D., Saeland, S., Davoust, J., Malissen, B., 2005. Dynamics and Function of Langerhans Cells In Vivo. Immunity 22, 643–654. https://doi.org/10.1016/j.immuni.2005.04.004

Kolter, J., Feuerstein, R., Zeis, P., Hagemeyer, N., Paterson, N., d'Errico, P., Baasch, S., Amann, L., Masuda, T., Lösslein, A., Gharun, K., Meyer-Luehmann, M., Waskow, C., Franzke, C.-W., Grün, D., Lämmermann, T., Prinz, M., Henneke, P., 2019. A Subset of Skin Macrophages Contributes to the Surveillance and Regeneration of Local Nerves. Immunity 50, 1482-1497.e7. https://doi.org/10.1016/j.immuni.2019.05.009

Kvedaraite, E., Milne, P., Khalilnezhad, A., Chevrier, M., Sethi, R., Lee, H.K., Hagey, D.W., von Bahr Greenwood, T., Mouratidou, N., Jädersten, M., Lee, N.Y.S., Minnerup, L., Tan, Y., Dutertre, C.-A., Benac, N., Hwang, Y.Y., Lum, J., Loh, A.H.P., Jansson, J., Teng, K.W.W., Khalilnezhad, S., Xu, W., Resteu, A., Tey, H.L., Guan, N.L., Larbi, A., Howland, S.W., Arnell, H., Andaloussi, S.E.L., Braier, J., Rassidakis, G., Galluzzo, L., Dzionek, A., Henter, J.-I., Chen, J., Collin, M., Ginhoux, F., 2022. Notch-dependent cooperativity between myeloid lineages promotes Langerhans cell histiocytosis pathology. Sci. Immunol. 7, eadd3330. https://doi.org/10.1126/sciimmunol.add3330

Kwok, I., Becht, E., Xia, Y., Ng, M., Teh, Y.C., Tan, L., Evrard, M., Li, J.L.Y., Tran, H.T.N., Tan, Y., Liu, D., Mishra, A., Liong, K.H., Leong, K., Zhang, Y., Olsson, A., Mantri, C.K., Shyamsunder, P., Liu, Z., Piot, C., Dutertre, C.-A., Cheng, H., Bari, S., Ang, N., Biswas, S.K., Koeffler, H.P., Tey, H.L., Larbi, A., Su, I.-H., Lee, B., St. John, A., Chan, J.K.Y., Hwang, W.Y.K., Chen, J., Salomonis, N., Chong, S.Z., Grimes, H.L., Liu, B., Hidalgo, A., Newell, E.W., Cheng, T., Ginhoux, F., Ng, L.G., 2020. Combinatorial Single-Cell Analyses of Granulocyte-Monocyte Progenitor Heterogeneity Reveals an Early Uni-potent Neutrophil Progenitor. Immunity 53, 303-318.e5. https://doi.org/10.1016/j.immuni.2020.06.005

La Manno, G., Soldatov, R., Zeisel, A., Braun, E., Hochgerner, H., Petukhov, V., Lidschreiber, K., Kastriti, M.E., Lönnerberg, P., Furlan, A., Fan, J., Borm, L.E., Liu, Z., van Bruggen, D., Guo, J., He, X., Barker, R., Sundström, E., Castelo-Branco, G., Cramer, P., Adameyko, I., Linnarsson, S., Kharchenko, P.V., 2018. RNA velocity of single cells. Nature 560, 494–498. https://doi.org/10.1038/s41586-018-0414-6

Lavin, Y., Winter, D., Blecher-Gonen, R., David, E., Keren-Shaul, H., Merad, M., Jung, S., Amit, I., 2014. Tissue-Resident Macrophage Enhancer Landscapes Are Shaped by the Local Microenvironment. Cell 159, 1312–1326. https://doi.org/10.1016/j.cell.2014.11.018

Lengqvist, J., Mata De Urquiza, A., Bergman, A.-C., Willson, T.M., Sjövall, J., Perlmann, T., Griffiths, W.J., 2004. Polyunsaturated Fatty Acids Including Docosahexaenoic and Arachidonic Acid Bind to the Retinoid X Receptor α Ligand-binding Domain. Mol. Cell. Proteomics 3, 692–703. https://doi.org/10.1074/mcp.M400003-MCP200

Liu, T.-T., Kim, S., Desai, P., Kim, D.-H., Huang, X., Ferris, S.T., Wu, R., Ou, F., Egawa, T., Van Dyken, S.J., Diamond, M.S., Johnson, P.F., Kubo, M., Murphy, T.L., Murphy, K.M., 2022. Ablation of cDC2 development by triple mutations within the Zeb2 enhancer. Nature 607, 142–148. https://doi.org/10.1038/s41586-022-04866-z

Liu, Xiaochun, Zhu, R., Luo, Y., Wang, S., Zhao, Y., Qiu, Z., Zhang, Y., Liu, Xiao, Yao, X., Li, X., Li, W., 2021. Distinct human Langerhans cell subsets orchestrate reciprocal functions and require different developmental regulation. Immunity 54, 2305-2320.e11. https://doi.org/10.1016/j.immuni.2021.08.012

Love, M.I., Huber, W., Anders, S., 2014. Moderated estimation of fold change and dispersion for RNA-seq data with DESeq2. Genome Biol. 15, 550. https://doi.org/10.1186/s13059-014-0550-8

Lutz, M.B., Strobl, H., Schuler, G., Romani, N., 2017. GM-CSF Monocyte-Derived Cells and Langerhans Cells As Part of the Dendritic Cell Family. Front. Immunol. 8, 1388. https://doi.org/10.3389/fimmu.2017.01388

Mass, E., Ballesteros, I., Farlik, M., Halbritter, F., Günther, P., Crozet, L., Jacome-Galarza, C.E., Händler, K., Klughammer, J., Kobayashi, Y., Gomez-Perdiguero, E., Schultze, J.L., Beyer, M., Bock, C., Geissmann, F., 2016. Specification of tissue-resident macrophages during organogenesis. Science 353, aaf4238. https://doi.org/10.1126/science.aaf4238

McCowan, J., Fercoq, F., Kirkwood, P.M., T'Jonck, W., Hegarty, L.M., Mawer, C.M., Cunningham, R., Mirchandani, A.S., Hoy, A., Humphries, D.C., Jones, G.-R., Hansen, C.G., Hirani, N., Jenkins, S.J., Henri, S., Malissen, B., Walmsley, S.R., Dockrell, D.H., Saunders, P.T.K., Carlin, L.M., Bain, C.C., 2021. The transcription factor EGR2 is indispensable for tissue-specific imprinting of alveolar macrophages in health and tissue repair. Sci. Immunol. 6, eabj2132. https://doi.org/10.1126/sciimmunol.abj2132

Meindl, S., Vaculik, C., Meingassner, J.G., Kramer, G., Akgün, J., Prior, M., Stuetz, A., Stingl, G., Elbe-Bürger, A., 2009. Differential Effects of Corticosteroids and Pimecrolimus on the Developing Skin Immune System in Humans and Mice. J. Invest. Dermatol. 129, 2184–2192. https://doi.org/10.1038/jid.2009.50

Melsted, P., Booeshaghi, A.S., Liu, L., Gao, F., Lu, L., Min, K.H., Da Veiga Beltrame, E., Hjörleifsson, K.E., Gehring, J., Pachter, L., 2021. Modular, efficient and constant-memory single-cell RNA-seq preprocessing. Nat. Biotechnol. 39, 813–818. https://doi.org/10.1038/s41587-021-00870-2

Merad, M., Hoffmann, P., Ranheim, E., Slaymaker, S., Manz, M.G., Lira, S.A., Charo, I., Cook, D.N., Weissman, I.L., Strober, S., Engleman, E.G., 2004. Depletion of host Langerhans cells before transplantation of donor alloreactive T cells prevents skin graft-versus-host disease. Nat. Med. 10, 510–517. https://doi.org/10.1038/nm1038

Merad, M., Manz, M.G., Karsunky, H., Wagers, A., Peters, W., Charo, I., Weissman, I.L., Cyster, J.G., Engleman, E.G., 2002. Langerhans cells renew in the skin throughout life under steady-state conditions. Nat. Immunol. 3, 1135–1141. https://doi.org/10.1038/ni852

Mielcarek, M., Kirkorian, A.Y., Hackman, R.C., Price, J., Storer, B.E., Wood, B.L., Leboeuf, M., Bogunovic, M., Storb, R., Inamoto, Y., Flowers, M.E., Martin, P.J., Collin, M., Merad, M., 2014. Langerhans Cell Homeostasis and Turnover After Nonmyeloablative and Myeloablative Allogeneic Hematopoietic Cell Transplantation. Transplantation 98, 563–568. https://doi.org/10.1097/TP.0000000000000097

Mohammed, J., Beura, L.K., Bobr, A., Astry, B., Chicoine, B., Kashem, S.W., Welty, N.E., Igyártó, B.Z., Wijeyesinghe, S., Thompson, E.A., Matte, C., Bartholin, L., Kaplan, A., Sheppard, D., Bridges, A.G., Shlomchik, W.D., Masopust, D., Kaplan, D.H., 2016. Stromal cells control the epithelial residence of DCs and memory T cells by regulated activation of TGF-β. Nat. Immunol. 17, 414–421. https://doi.org/10.1038/ni.3396

Nagao, K., Kobayashi, T., Moro, K., Ohyama, M., Adachi, T., Kitashima, D.Y., Ueha, S., Horiuchi, K., Tanizaki, H., Kabashima, K., Kubo, A., Cho, Y., Clausen, B.E., Matsushima, K., Suematsu, M., Furtado, G.C., Lira, S.A., Farber, J.M., Udey, M.C., Amagai, M., 2012. Stress-induced production of chemokines by hair follicles regulates the trafficking of dendritic cells in skin. Nat. Immunol. 13, 744–752. https://doi.org/10.1038/ni.2353

Platzer, B., Richter, S., Kneidinger, D., Waltenberger, D., Woisetschläger, M., Strobl, H., 2009. Aryl Hydrocarbon Receptor Activation Inhibits In Vitro Differentiation of Human Monocytes and Langerhans Dendritic Cells. J. Immunol. 183, 66–74. https://doi.org/10.4049/jimmunol.0802997

Polak, M.E., Singh, H., 2021. Tolerogenic and immunogenic states of Langerhans cells are orchestrated by epidermal signals acting on a core maturation gene module. BioEssays 43, 2000182. https://doi.org/10.1002/bies.202000182

Rannug, A., Fritsche, E., 2006. The aryl hydrocarbon receptor and light. Biol. Chem. 387. https://doi.org/10.1515/BC.2006.143

Reynolds, G., Vegh, P., Fletcher, J., Poyner, E.F.M., Stephenson, E., Goh, I., Botting, R.A., Huang, N., Olabi, B., Dubois, A., Dixon, D., Green, K., Maunder, D., Engelbert, J., Efremova, M., Polański, K., Jardine, L., Jones, C., Ness, T., Horsfall, D., McGrath, J., Carey, C., Popescu, D.-M., Webb, S., Wang, X., Sayer, B., Park, J.-E., Negri, V.A., Belokhvostova, D., Lynch, M.D., McDonald, D., Filby, A., Hagai, T., Meyer, K.B., Husain, A., Coxhead, J., Vento-Tormo, R., Behjati, S., Lisgo, S., Villani, A.-C., Bacardit, J., Jones, P.H., O'Toole, E.A., Ogg, G.S., Rajan, N., Reynolds, N.J., Teichmann, S.A., Watt, F.M., Haniffa, M., 2021. Developmental cell programs are co-opted in inflammatory skin disease. Science 371, eaba6500. https://doi.org/10.1126/science.aba6500

Santos e Sousa, P., Ciré, S., Conlan, T., Jardine, L., Tkacz, C., Ferrer, I.R., Lomas, C., Ward, S., West, H., Dertschnig, S., Blobner, S., Means, T.K., Henderson, S., Kaplan, D.H., Collin, M., Plagnol, V., Bennett, C.L., Chakraverty, R., 2018. Peripheral tissues reprogram CD8+ T cells for pathogenicity during graft-versus-host disease. JCI Insight 3, e97011. https://doi.org/10.1172/jci.insight.97011

Schaerli, P., Willimann, K., Ebert, L.M., Walz, A., Moser, B., 2005. Cutaneous CXCL14 Targets Blood Precursors to Epidermal Niches for Langerhans Cell Differentiation. Immunity 23, 331–342. https://doi.org/10.1016/j.immuni.2005.08.012

Schmidt, J.V., Su, G.H., Reddy, J.K., Simon, M.C., Bradfield, C.A., 1996. Characterization of a murine Ahr null allele: involvement of the Ah receptor in hepatic growth and development. Proc. Natl. Acad. Sci. 93, 6731–6736. https://doi.org/10.1073/pnas.93.13.6731

Schulz, C., Perdiguero, E.G., Chorro, L., Szabo-Rogers, H., Cagnard, N., Kierdorf, K., Prinz, M., Wu, B., Jacobsen, S.E.W., Pollard, J.W., Frampton, J., Liu, K.J., Geissmann, F., 2012. A Lineage of Myeloid Cells Independent of Myb and Hematopoietic Stem Cells. Science 336, 86–90. https://doi.org/10.1126/science.1219179

Scott, C.L., T'Jonck, W., Martens, L., Todorov, H., Sichien, D., Soen, B., Bonnardel, J., De Prijck, S., Vandamme, N., Cannoodt, R., Saelens, W., Vanneste, B., Toussaint, W., De Bleser, P., Takahashi, N., Vandenabeele, P., Henri, S., Pridans, C., Hume, D.A., Lambrecht, B.N., De Baetselier, P., Milling, S.W.F., Van Ginderachter, J.A., Malissen, B., Berx, G., Beschin, A., Saeys, Y., Guilliams, M., 2018. The Transcription Factor ZEB2 Is Required to Maintain the Tissue-Specific Identities of Macrophages. Immunity 49, 312-325.e5. https://doi.org/10.1016/j.immuni.2018.07.004

Seré, K., Baek, J.-H., Ober-Blöbaum, J., Müller-Newen, G., Tacke, F., Yokota, Y., Zenke, M., Hieronymus, T., 2012. Two Distinct Types of Langerhans Cells Populate the Skin during Steady State and Inflammation. Immunity 37, 905–916. https://doi.org/10.1016/j.immuni.2012.07.019

Sirvent, S., Vallejo, A.F., Davies, J., Clayton, K., Wu, Z., Woo, J., Riddell, J., Chaudhri, V.K., Stumpf, P., Nazlamova, L.A., Wheway, G., Rose-Zerilli, M., West, J., Pujato, M., Chen, X., Woelk, C.H., MacArthur, B., Ardern-Jones, M., Friedmann, P.S., Weirauch, M.T., Singh, H., Polak, M.E., 2020. Genomic programming of IRF4-expressing human Langerhans cells. Nat. Commun. 11, 313. https://doi.org/10.1038/s41467-019-14125-x

Stockinger, B., 2009. Beyond toxicity: aryl hydrocarbon receptor-mediated functions in the immune system. J. Biol. 8, 61. https://doi.org/10.1186/jbiol170

Street, K., Risso, D., Fletcher, R.B., Das, D., Ngai, J., Yosef, N., Purdom, E., Dudoit, S., 2018. Slingshot: cell lineage and pseudotime inference for single-cell transcriptomics. BMC Genomics 19, 477. https://doi.org/10.1186/s12864-018-4772-0

Strobl, H., Krump, C., Borek, I., 2019. Micro-environmental signals directing human epidermal Langerhans cell differentiation. Semin. Cell Dev. Biol. 86, 36–43. https://doi.org/10.1016/j.semcdb.2018.02.016

Stuart, T., Butler, A., Hoffman, P., Hafemeister, C., Papalexi, E., Mauck, W.M., Hao, Y., Stoeckius, M., Smibert, P., Satija, R., 2019. Comprehensive Integration of Single-Cell Data. Cell 177, 1888-1902.e21. https://doi.org/10.1016/j.cell.2019.05.031

Subach, O.M., Cranfill, P.J., Davidson, M.W., Verkhusha, V.V., 2011. An Enhanced Monomeric Blue Fluorescent Protein with the High Chemical Stability of the Chromophore. PLoS ONE 6, e28674. https://doi.org/10.1371/journal.pone.0028674

Tabib, Y., Jaber, N.S., Nassar, M., Capucha, T., Mizraji, G., Nir, T., Koren, N., Aizenbud, I., Maimon, A., Eli-Berchoer, L., Wilensky, A., Burstyn-Cohen, T., Hovav, A.-H., 2018. Cell-intrinsic regulation of murine epidermal Langerhans cells by protein S. Proc. Natl. Acad. Sci. 115. https://doi.org/10.1073/pnas.1800303115

Tacke, F., Alvarez, D., Kaplan, T.J., Jakubzick, C., Spanbroek, R., Llodra, J., Garin, A., Liu, J., Mack, M., van Rooijen, N., Lira, S.A., Habenicht, A.J., Randolph, G.J., 2007. Monocyte subsets differentially employ CCR2, CCR5, and CX3CR1 to accumulate within atherosclerotic plaques. J. Clin. Invest. 117, 185–194. https://doi.org/10.1172/JCI28549

Thiele, I., Swainston, N., Fleming, R.M.T., Hoppe, A., Sahoo, S., Aurich, M.K., Haraldsdottir, H., Mo, M.L., Rolfsson, O., Stobbe, M.D., Thorleifsson, S.G., Agren, R., Bölling, C., Bordel, S., Chavali, A.K., Dobson, P., Dunn, W.B., Endler, L., Hala, D., Hucka, M., Hull, D., Jameson, D., Jamshidi, N., Jonsson, J.J., Juty, N., Keating, S., Nookaew, I., Le Novère, N., Malys, N., Mazein, A., Papin, J.A., Price, N.D., Selkov, E., Sigurdsson, M.I., Simeonidis, E., Sonnenschein, N., Smallbone, K., Sorokin, A., van Beek, J.H.G.M., Weichart, D., Goryanin, I., Nielsen, J., Westerhoff, H.V., Kell, D.B., Mendes, P., Palsson, B.Ø., 2013. A community-driven global reconstruction of human metabolism. Nat. Biotechnol. 31, 419–425. https://doi.org/10.1038/nbt.2488

T'Jonck, W., Guilliams, M., Bonnardel, J., 2018. Niche signals and transcription factors involved in tissue-resident macrophage development. Cell. Immunol. 330, 43–53. https://doi.org/10.1016/j.cellimm.2018.02.005

Toubai, T., Tawara, I., Sun, Y., Liu, C., Nieves, E., Evers, R., Friedman, T., Korngold, R., Reddy, P., 2012. Induction of acute GVHD by sex-mismatched H-Y antigens in the absence of functional radiosensitive host hematopoietic–derived antigen-presenting cells. Blood 119, 3844–3853. https://doi.org/10.1182/blood-2011-10-384057

Tripp, C.H., Chang-Rodriguez, S., Stoitzner, P., Holzmann, S., Stössel, H., Douillard, P., Saeland, S., Koch, F., Elbe-Bürger, A., Romani, N., 2004. Ontogeny of Langerin/CD207 Expression in the Epidermis of Mice. J. Invest. Dermatol. 122, 670–672. https://doi.org/10.1111/j.0022-202X.2004.22337.x

Trzebanski, S., Kim, J.-S., Larossi, N., Kancheva, D., Bastos, J., Haddad, M., Aizik, D., Kralova, J., Gross-Vered, M., Halfon, S.B.-, Lapidot, T., Alon, R., Movahedi, K., Jung, S., 2023. Murine classical monocyte subsets display distinct functions and fates. https://doi.org/10.1101/2023.07.29.551083

Valujskikh, A., Lantz, O., Celli, S., Matzinger, P., Heeger, P.S., 2002. Cross-primed CD8+ T cells mediate graft rejection via a distinct effector pathway. Nat. Immunol. 3, 844–851. https://doi.org/10.1038/ni831

Viola, M.F., Chavero-Pieres, M., Modave, E., Delfini, M., Stakenborg, N., Estévez, M.C., Fabre, N., Appeltans, I., Martens, T., Vandereyken, K., Theobald, H., Van Herck, J., Petry, P., Verheijden, S., De Schepper, S., Sifrim, A., Liu, Z., Ginhoux, F., Azhar, M., Schlitzer, A., Matteoli, G., Kierdorf, K., Prinz, M., Vanden Berghe, P., Voet, T., Boeckxstaens, G., 2023. Dedicated macrophages organize and maintain the enteric nervous system. Nature 618, 818–826. https://doi.org/10.1038/s41586-023-06200-7

Wagner, A., Wang, C., Fessler, J., DeTomaso, D., Avila-Pacheco, J., Kaminski, J., Zaghouani, S., Christian, E., Thakore, P., Schellhaass, B., Akama-Garren, E., Pierce, K., Singh, V., Ron-Harel, N., Douglas, V.P., Bod, L., Schnell, A., Puleston, D., Sobel, R.A., Haigis, M., Pearce, E.L., Soleimani, M., Clish, C., Regev, A., Kuchroo, V.K., Yosef, N., 2021. Metabolic modeling of single Th17 cells reveals regulators of autoimmunity. Cell 184, 4168-4185.e21. https://doi.org/10.1016/j.cell.2021.05.045

Walker, J.A., Clark, P.A., Crisp, A., Barlow, J.L., Szeto, A., Ferreira, A.C.F., Rana, B.M.J., Jolin, H.E., Rodriguez-Rodriguez, N., Sivasubramaniam, M., Pannell, R., Cruickshank, J., Daly, M., Haim-Vilmovsky, L., Teichmann, S.A., McKenzie, A.N.J., 2019. Polychromic Reporter Mice Reveal Unappreciated Innate Lymphoid Cell Progenitor Heterogeneity and Elusive ILC3 Progenitors in Bone Marrow. Immunity 51, 104-118.e7. https://doi.org/10.1016/j.immuni.2019.05.002

Wang, Y., Szretter, K.J., Vermi, W., Gilfillan, S., Rossini, C., Cella, M., Barrow, A.D., Diamond, M.S., Colonna, M., 2012. IL-34 is a tissue-restricted ligand of CSF1R required for the development of Langerhans cells and microglia. Nat. Immunol. 13, 753–760. https://doi.org/10.1038/ni.2360

Wasko, R., Bridges, K., Pannone, R., Sidhu, I., Xing, Y., Naik, S., Miller-Jensen, K., Horsley, V., 2022. Langerhans cells are essential components of the angiogenic niche during murine skin repair. Dev. Cell 57, 2699-2713.e5. https://doi.org/10.1016/j.devcel.2022.11.012

Wculek, S.K., Heras-Murillo, I., Mastrangelo, A., Mañanes, D., Galán, M., Miguel, V., Curtabbi, A., Barbas, C., Chandel, N.S., Enríquez, J.A., Lamas, S., Sancho, D., 2023. Oxidative phosphorylation selectively orchestrates tissue macrophage homeostasis. Immunity 56, 516-530.e9. https://doi.org/10.1016/j.immuni.2023.01.011

West, H.C., Davies, J., Henderson, S., Adegun, O.K., Ward, S., Ferrer, I.R., Tye, C.A., Vallejo, A.F., Jardine, L., Collin, M., Polak, M.E., Bennett, C.L., 2022. Loss of T cell tolerance in the skin following immunopathology is linked to failed restoration of the dermal niche by recruited macrophages. Cell Rep. 39, 110819. https://doi.org/10.1016/j.celrep.2022.110819

Wu, X., Briseño, C.G., Durai, V., Albring, J.C., Haldar, M., Bagadia, P., Kim, K.-W., Randolph, G.J., Murphy, T.L., Murphy, K.M., 2016. Mafb lineage tracing to distinguish macrophages from other immune lineages reveals dual identity of Langerhans cells. J. Exp. Med. 213, 2553–2565. https://doi.org/10.1084/jem.20160600

Yáñez, A., Coetzee, S.G., Olsson, A., Muench, D.E., Berman, B.P., Hazelett, D.J., Salomonis, N., Grimes, H.L., Goodridge, H.S., 2017. Granulocyte-Monocyte Progenitors and Monocyte-Dendritic Cell Progenitors Independently Produce Functionally Distinct Monocytes. Immunity 47, 890-902.e4. https://doi.org/10.1016/j.immuni.2017.10.021

Zhang, S., Edwards, T.N., Chaudhri, V.K., Wu, J., Cohen, J.A., Hirai, T., Rittenhouse, N., Schmitz, E.G., Zhou, P.Y., McNeil, B.D., Yang, Y., Koerber, H.R., Sumpter, T.L., Poholek, A.C., Davis, B.M., Albers, K.M., Singh, H., Kaplan, D.H., 2021. Nonpeptidergic neurons suppress mast cells via glutamate to maintain skin homeostasis. Cell 184, 2151-2166.e16. https://doi.org/10.1016/j.cell.2021.03.002

ACKNOWLEDGEMENTS

We thank the UCL Biological Services for their support with animal work. We are grateful to Carlos Minutti and Caetano Reis e Sousa support with reagents and experimental advice. This study was funded by Biotechnology and Biological Sciences Research Council grant BB/T005246/1 (A.A., J.D. and C.L.B.). Acquisition and analysis of human perinatal samples, MEP, SS were funded by the Wellcome Trust Sir Henry Dale Fellowship 109377/Z/15/Z.

Conflicts of interest, MEP is currently employed at Johnson and Johnson Innovative Medicine. Johnson and Johnson Innovative Medicine or any of employees/stakeholders have not been involved in any part or aspect of the project or manuscript.

Conceptualization, C.L.B., M.E.P.; Methodology, A.A., J.D., S.S., S.H., S.T., J.S., M.L.L., I.B.C., S.M.M, E.E. and S.J; Investigation, A.A., J.D., S.S.; Formal analysis, S.S., S.H. and M.E.P, A. V; Resources: C.M., A. V., N.J.H., M. A-J.; Writing - Original Draft, C.L.B and M.E.P; Writing - Review and Editing, A.A., S.H., S.M.M, E.E., S. J., M. A-J, M.E.P and C.L.B; Funding Acquisition and supervision, C.L.B and M.E.P.
Data and materials are available upon request.